B. TECH. PROJECT REPORT

On

Response of carbon fiber reinforced composite under high strain rates

BY

Aman Patel

Piyush Singh

Sagar Gome

DISCIPLINE OF CIVIL ENGINEERING

INDIAN INSTITUTE OF TECHNOLOGY INDORE

NOVEMBER 2019

Response of carbon fiber reinforced composite under high strain rates

A PROJECT REPORT

Submitted in partial fulfillment of the requirements for the award of the degrees

of

BACHELOR OF TECHNOLOGY
in

CIVIL ENGINEERING

Submitted by:
Aman Patel
Piyush Singh
Sagar Gome

Guided by:
Dr. Abhishek Rajput
Asst. Professor
(Department of Civil Engineering)

INDIAN INSTITUTE OF TECHNOLOGY INDORE

NOVEMBER 2019

CANDIDATE'S DECLARATION

We hereby declare that the project entitled **"Response of carbon fiber reinforced composite under high strain rates"** submitted in partial fulfillment for the award of the degree of Bachelor of Technology in 'Civil Engineering' completed under the supervision of **Dr. Abhishek Rajput, Assistant Professor, Department of Civil Engineering,** IIT Indore is an authentic work.

Further, we declare that we have not submitted this work for the award of any other degree elsewhere.

Signature and name of the student(s) with date

CERTIFICATE by BTP Guide(s)

It is certified that the above statement made by the students is correct to the best of my/our knowledge.

Signature of BTP Guide(s) with dates and their designation

Preface

This report on “**Response of carbon fiber reinforced composite under high strain rates** " is prepared under the guidance of **Dr. Abhishek Rajput**.

Through this report we have attempted to give a detailed plan of inventive finite element model with the damage model specifically implemented for CFRP. More emphasis is made on understanding the perforation process and its application as well as on assessment of perforation characteristics.

We have tried to the best of our abilities and knowledge to explain the content in a lucid manner. We have also added models, reference images, relevant graphs, tables, photos and figures to make it more illustrative.

Aman Patel
Piyush Singh
Sagar Gome

B.Tech. IV Year
Discipline of Civil Engineering
IIT Indore

Acknowledgements

We wish to thank Dr. Abhishek Rajput for his kind support and valuable guidance. He was always available for the discussion, to answer our doubts, to guide us with the software modelling and help us in moving forward with the project through different phases. He provided an environment where we were motivated to discuss new ideas and our problems.

We would also like to acknowledge Dr. Asharf Iqbal, Associate Professor, IIT Roorkee for giving us sincere cooperation and guidance in carrying out the experiment, due to that we were able to complete our research.

Without his support this report would not have been possible.

Aman Patel
Piyush Singh
Sagar Gome

B.Tech. IV Year
Discipline of Civil Engineering
IIT Indore

Abstract

Carbon fibre composite has great potential as protective material because of its unique high strength proving to be of high interest against impact analysis in the market. In this study, practical and numerical simulation was done by damage response model on CFRP created under ABAQUS software using Hashin's criteria. It works on impact perforation of CFRP laminates impacted with steel bullet travelling at velocities between 50m/s to 300m/s has been performed.

The work basically focuses on two major subjects in impact perforation studies which is the assessment of perforation characteristics and understanding of the perforation process and its applications. The targeted plate is made up of carbon fibre–reinforced polymer composites whereas impactor are made up of steel projectiles having different nose angles, with CRH 1.5 and CRH 2 and also hemispherical.

The ballistic limit, residual velocity and perforation energy predicted from the numerical models with experimental data obtained from testing. After obtaining the data, the perforation mechanism was analyzed based on numerical and experimental observation. So in our study, we have provided state-of-the-art information in the fast-growing field of impact analysis of CFRP by alluding to various literature.

TABLE OF CONTENT

LIST OF TABLES

LIST OF FIGURES

Figure

Chapter 1: Introduction

1.1 What is CFRP?

Carbon Fibre reinforced polymer (CFRP) are extremely strong and light fibre consists of carbon fibre used for the manufacturing of many products being helpful to us in our daily life. It is a term used to describe a fibre-reinforced composite material which consists of two parts:

a) Reinforcement:

Carbon fibre acts as reinforcing material which provides the strength and rigidity measured by stress and elastic modulus.

Figure 1.1: Raw carbon fibre

b) Matrix

Synthetic resin as the matrix like epoxy which is used to bind the reinforcements together. Epoxy is basically thermoset resins-polymers that is made from curing liquid polymer into the irreversibly hardened materials. These epoxies provide certain benefits in manufacturing composite parts such as:-

- High Adaptability
- High Strength
- Exceptional Adhesion properties
- Low shrinkage
- Toughness and impact resistance.

Unlike conventional engineering materials like steel, aluminum etc. which shows isotropic properties, CFRP shows directional properties. The properties of CFRP depends on the proportion of carbon fibre relative to the polymer and also the layout of carbon fibres.

1.2 Why Choose CFRP?

Carbon fibre has been used since ancient Egyptian times where straws in clays were used as alternatives for building. In present-day times the utilization of composite materials ranges from civil to aviation applications that offer several benefits to improve the quality of products such as:

- Exceptionally high strength to weight ratio.
- Resistance to fatigue
- High tensile strength
- Fabrication flexibility and design of composite materials like
    - The requirement of less assembly time and raw materials.
    - Decrease the number of parts required.
- Resist temperature extremes, wear and corrosion.

1.3 Where carbon fibre is mostly used?

A wide assortment of industries esteem carbon fibre for the above advantages, and it shows up in a wide range of uses. A portion of these materials' most prevalent uses include:

a) Aerospace Industries:

High modulus of carbon fibre serves a huge replacement option for traditional alloys like aluminum, titanium etc. has taken the industries by storm because of its lightweight helping in fuel consumption in new aircraft like Boeing 787 Dreamliner.

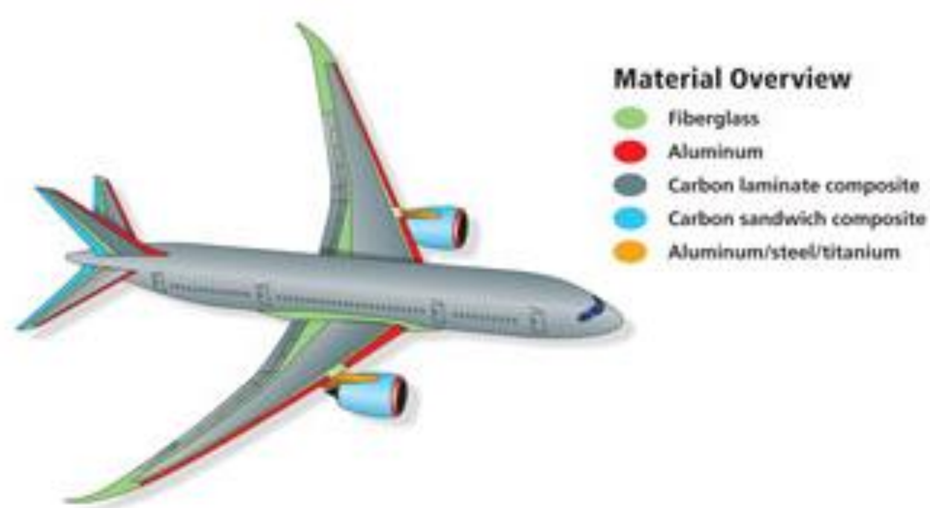

Figure 1.2: Figure showing material composition of Boeing 787 Dreamliner

b) **Sporting Goods and Domestic use:**

Racquets, softball bats, hockey sticks etc. are frequently made of carbon fibre which helps in preserving durability. At the same time, carbon fibre furniture and appliances give beautiful appeal without sacrificing quality.

Figure 1.3: Sports items made of carbon fibre

c) **Automotive Engineering:**

Manufactures of the high-end car company and race cars have been using carbon fibres capacity to increase the aesthetic appeal of their products without weighing down their equipment.

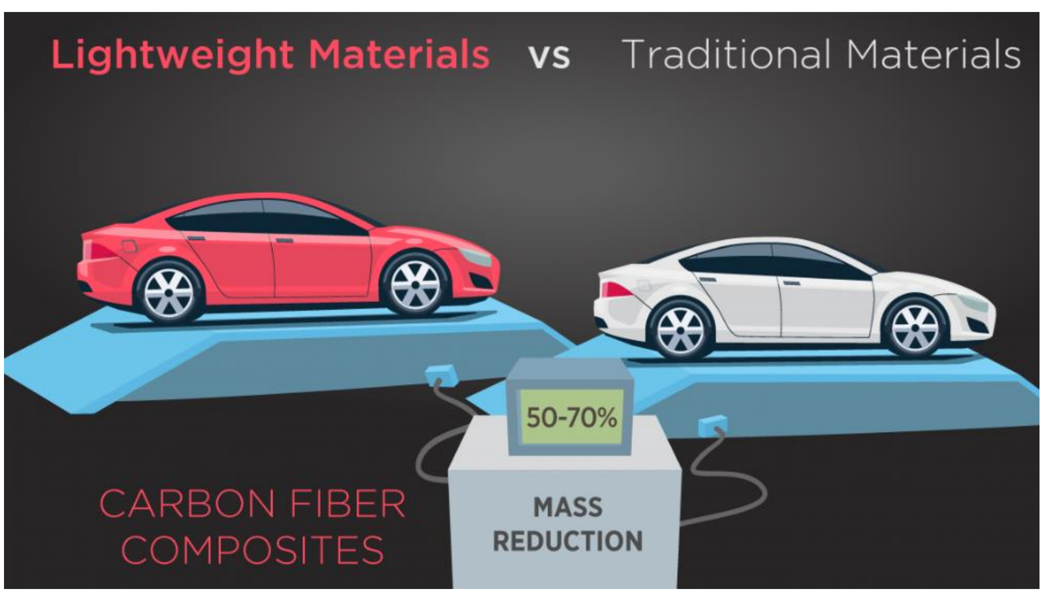

Figure 1.4: Figure showing carbon fibre impact on reducing weight.

1.4 Disadvantages of using CFRP composites:

- **Cost:** Depending upon the present economic situations, the sort of carbon fibre, and the fibre tow size, the cost of carbon fibre can change significantly. This disparity is even greater when comparing steel with CFRP composites.

- Temperature and humidity can have profound effects on CFRPs.

- CFRPs display strong corrosion resistance although the impact of moisture at wide scopes of temperatures can prompt to degradation of the mechanical properties of CFRPs, especially at the matrix fibre interface.

1.5 Current studies and research gap:

Research has been done on the high velocity perforation mechanism and its characteristics on Kevlar/polyester composite laminates by kasano [10] and similar assessment was done on carbon composite laminate by Goldsmith,1995 [12] but the perforation criteria was not covered and some results where absurd. Impact damage evaluation and fracture analysis was observed using Non-destructive radiography (NDT) but was performed on low velocity by shi[4]. Also recent research on CFRP using finite element 3D damage model using ABAQUS was performed but the focus was entirely on ripping mechanism by Pederson[8].

1.6 Our Objective:

- The research on CFRP has been focused on composite-sandwich with different material but not on entirely CFRP impacted with high velocity. The purpose of this work is to determine the perforation characteristics of carbon fibre composite laminates both analytically and experimentally struck by steel made bullet of a different shape. High-velocity impact by steel bullet projectile on orthotropic CFRP composite laminates is investigated. It comprises of an experimental part wherein impact tests has been performed in a wide range of velocities from 50m/s till the ballistic range of 300m/s. It was helpful in determining ballistics limit velocities, residual velocities and perforation energy. We have moreover worked on a finite element model in which a damage model explicitly for CFRP has been implemented. Numerical simulation was performed and experimental tests was carried out in IIT Roorkee to have better insight of our objective of understanding perforation mechanism of carbon fibre under high strain-rate.

CHAPTER 2: Impact Model for Composite Damage

Analysis of CFRP/epoxy composites plate was carried first through numerical simulation in ABAQUS and then the experimental test was carried out. Failure mode implemented in fibre is explained using Damage Models. Damage occurs in two phases: damage initiation and damage evolution.

2.1 Damage Modeling:

The unidirectional fibre composite was simulated with an orthotropic damage elastic model. The stress-strain relationship for this composite is shown below in equation 1:

$$\begin{pmatrix} \sigma_{11} \\ \sigma_{22} \\ \sigma_{33} \\ \sigma_{12} \\ \sigma_{23} \\ \sigma_{31} \end{pmatrix} = \begin{pmatrix} C_{11} & C_{12} & C_{13} & 0 & 0 & 0 \\ C_{12} & C_{22} & C_{23} & 0 & 0 & 0 \\ C_{13} & C_{23} & C_{33} & 0 & 0 & 0 \\ 0 & 0 & 0 & 2G_{12} & 0 & 0 \\ 0 & 0 & 0 & 0 & 2G_{23} & 0 \\ 0 & 0 & 0 & 0 & 0 & 2G_{31} \end{pmatrix} \begin{pmatrix} \varepsilon_{11} \\ \varepsilon_{22} \\ \varepsilon_{22} \\ \varepsilon_{12} \\ \varepsilon_{23} \\ \varepsilon_{31} \end{pmatrix} \tag{1}$$

Where the undamaged constants are

$$C^{\circ}_{11} = E^{\circ}_{11}(1-\upsilon_{23}\upsilon_{32})\Gamma \tag{2}$$

$$C^{\circ}_{22} = E^{\circ}_{22}(1-\upsilon_{13}\upsilon_{31})\Gamma \tag{3}$$

$$C^{\circ}_{33} = E^{\circ}_{33}(1-\upsilon_{12}\upsilon_{21})\Gamma \tag{4}$$

$$C^{\circ}_{12} = E^{\circ}_{11}(\upsilon_{21}+\upsilon_{31}\upsilon_{23})\Gamma \tag{5}$$

$$C^{\circ}_{23} = E^{\circ}_{22}(\upsilon_{32}+\upsilon_{12}\upsilon_{31})\Gamma \tag{6}$$

$$C^{\circ}_{13} = E^{\circ}_{11}(\upsilon_{31}+\upsilon_{21}\upsilon_{32})\Gamma \tag{7}$$

Where

$$\Gamma = 1/(1-\upsilon_{12}\upsilon_{21}-\upsilon_{23}\upsilon_{32}-\upsilon_{31}\upsilon_{13}-2\upsilon_{21}\upsilon_{32}\upsilon_{31}) \tag{8}$$

The global damage variables associated with fibre failure mode and the matrix failure mode is presented as d_f and d_m respectively. Global Damage variables are used in equation 9, 10 are d_{fc}, d_{ft}, d_{mc} and d_{mt} represented as fibre compression, fibre tension, matrix compression and matrix tension failure modes respectively:

$$d_f = 1-(1-d_{ft})(1-d_{fc}) \tag{9}$$

$$d_m = 1-(1-d_{mt})(1-d_{mc}) \tag{10}$$

Using equation 9, 10 with the constants in equation 2 to 7 as well as G12, G13 and G23 gives

$$C_{11} = (1-d_f)C^{\circ}_{11} \tag{11}$$

$$C_{22} = (1-d_f)(1-d_m)C^{\circ}_{22} \tag{12}$$

$$C_{33} = (1-d_f)(1-d_m)C^{\circ}_{33} \tag{13}$$

$$C_{12} = (1-d_f)(1-d_m)C^{\circ}_{12} \tag{14}$$

$$C_{23} = (1-d_f)(1-d_m)C^{\circ}_{23} \tag{15}$$

$$C_{13} = (1-d_f)(1-d_m)C^{\circ}_{13} \tag{16}$$

$$G_{12} = (1-d_f)(1-s_{mt}d_{mt})(1-s_{mc}d_{mc})G^{\circ}_{12} \tag{17}$$

$$G_{23} = (1-d_f)(1-s_{mt}d_{mt})(1-s_{mc}d_{mc})G^{\circ}_{23} \tag{18}$$

$$G_{31} = (1-d_f)(1-s_{mt}d_{mt})(1-s_{mc}d_{mc})G^{\circ}_{31} \tag{19}$$

The factors to help in controlling the shear stiffness loss due to the failure of the matrix in compression s_{mc} and tension s_{mt} are included in the last three equations.

2.2 Why modelling was done in ABAQUS/Explicit?

Because of the complexities of modelling contact and the nonlinearities that can be included, the model was designed using ABAQUS/Explicit than ABAQUS/Standard. Since ABAQUS/Standard uses Newton's Method, ABAQUS/Explicit works on explicit central-difference time integration method.

The term "Explicit" is used because the focus is on calculating velocities, acceleration and position of the next step from the current one. To make the model, system equations were placed into matrix form. The matrix of the global system of equation is formed by arranging the equations of the local system using node connectivity, streamlining the computations and improving the efficiency of the calculations. This makes a banded matrix, implying that the conditions are arranged such that all non-zero valves lay along the diagonal.

The explicit central-difference method requires extremely little increments be used, the bit of leeway being that the arrangement changes almost little for every augmentation, meaning the errors remain even considerably smaller. While an enormous number of increments are required, they will be in relatively easy computationally.

Flow-chart of this algorithm as shown in figure 2.1 where t is the specified step time; M is the mass matrix; u, ú and ü is displacements, velocities and accelerations respectively.

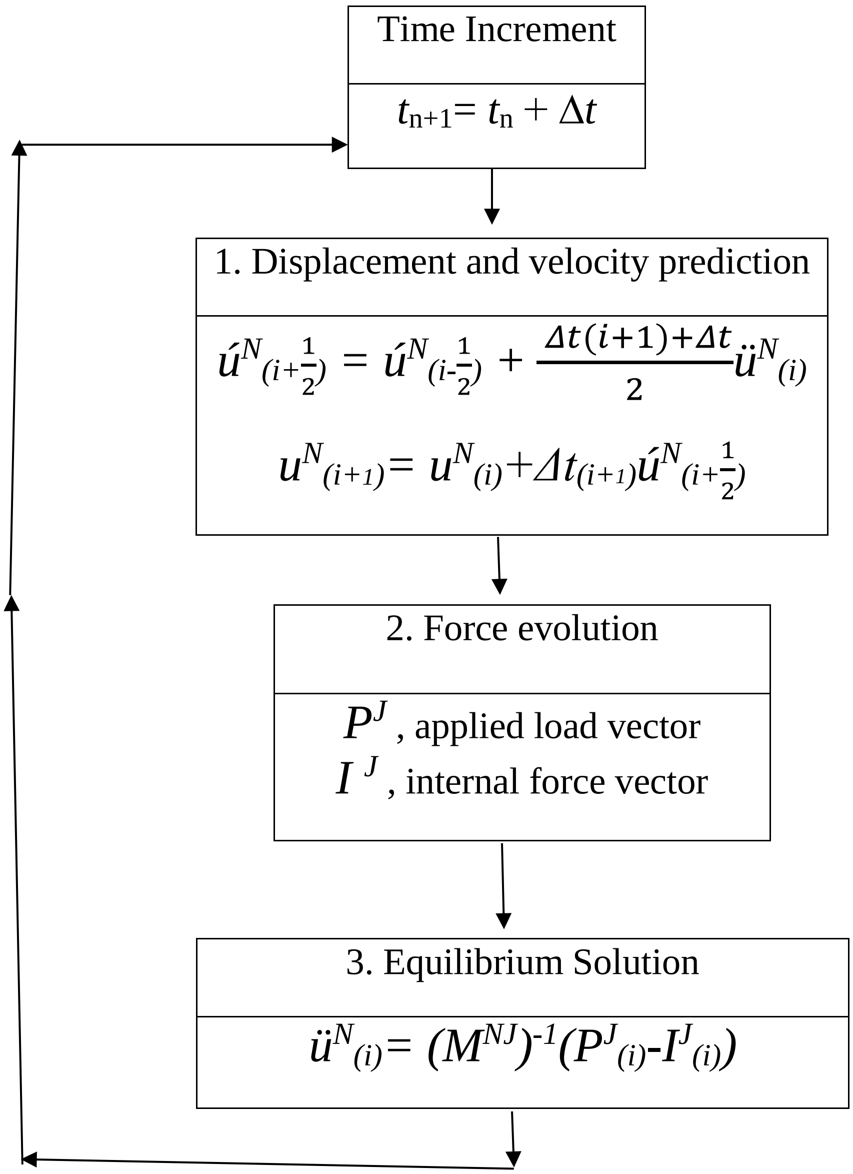

Figure 2.1 Explicit Central-Difference Time Integration

2.3 Damage Initiation Criteria: Damage modeling in laminate composites is visualized either by stress-strain based failure criteria or damage mechanics concepts. Hashin proposed failure criteria for composites to be implemented in the majority of finite element software.

- **Hashin Failure Theory:** Hashin by analyzing failure due to specific stress rates assumed the existence of a three-dimensional failure criterion by employing average stresses or strains. Hashin failure equation is quadratic in nature because of curve fitting is not physical in reasoning to material properties.

The general form of the equation is:

$$A_1I_1+B_1I_1^2+A_2I_2+B_2I_2^2+C_{12}I_1I_2+A_3I_3+A_4I_4=1 \tag{20}$$

Where,

$$I_1=\sigma_{11} \tag{21}$$

$$I_2=\sigma_{22}+\sigma_{33} \tag{22}$$

$$I_3=\sigma_{23}^2-\sigma_{22}\sigma_{33}=\frac{1}{4}(\sigma_{22}-\sigma_{33})+\sigma_{23}^2 \tag{23}$$

$$I_4=\sigma_{12}^2+\sigma_{13}^2 \tag{24}$$

To find out the constants A_1, A_2, A_3, A_4, B_1, B_2, C_1 we have to apply known stress into the equation. Pure transverse or axial shear loading is applied individually, A_3 and A_4 are the equation obtained as can be seen below:

$$A_3=\frac{1}{\tau_T^2} \tag{25}$$

$$A_4=\frac{1}{\tau_A^2} \tag{26}$$

The fibre failure is studied using with this loading, the matrix failure modes will be eliminated. The fibre modes are influenced by the stresses σ_{11}, σ_{12} and σ_{13} giving:

$$A_f\sigma_{11}+B_f\sigma_{11}^2+\frac{1}{\tau_A^2}(\sigma_{12}^2+\sigma_{13}^2)=1 \tag{27}$$

The equation can be approximated for tensile fibre influenced failure within an elliptical failure envelope is shown as:

$$\left(\frac{\sigma_{11}}{\sigma_A^+}\right)^2 + \frac{1}{\tau_A^2}(\sigma_{12}^2 + \sigma_{13}^2) = 1 \tag{28}$$

The ABAQUS gives a tensile fibre influenced failure criterion:

$$\left(\frac{\sigma_{11}}{X_{1t}}\right)^2 + \left(\frac{\sigma_{12}}{S_{12}}\right)^2 + \left(\frac{\sigma_{13}}{S_{13}}\right)^2 = 1 \tag{29}$$

When $X_{1t} = \sigma_A^+$ and $\tau_A = S_{12}$ and since isotropy has to be same such that

$S_{12} = S_{13}$, the equation (28) and (29) are the same.

- **Element Failure:** When the element reaches the failure point as determined by the model, the element status valve shifts from 1 to 0. Now after this the stress point of the material is zero and its significance to the model stiffness becomes nil. When all the point in the material has reached zero then model mesh removes the element.

Chapter 3: Materials Used

3.1 CFRP Sheets:

a) Manufacture: The essential component of CFRP is carbon fibre; this is created from a precursor polymer, for example, polyacrylonitrile (PAN), rayon, or petroleum pitch. The polymer is first spun into filament yarn using chemical and mechanical methods to first adjust the polymer chains in a way to enhance the final physical properties of the finished carbon fibre. After spinning, the polymer yarns are then heated to remove non-carbon atoms, giving the final carbon fibre. The fibres are further treated to improve handling qualities. From these fibres, the unidirectional sheet is created. Then these sheets are layered into the desired orientation required.

b) Specifications: In our simulation, we have taken CFRP sheets of 1mm and 2mm thick having dimensions of (200x200) mm and (300x300) mm for both dimension.

c) Properties: The material property of CFRP sheets used were determine by experimental test performed in labs and mentioned in the literature taken in our studies as

PROPERTY	**VALUE**
T300/5208 epoxy composites	
Longitudinal Modulus, E_{11} (GPa)	**136**
Transverse Modulus, E_{22} (GPa)	**9.8**
Out-of-plane Modulus, E_{33} (GPa)	**9.8**
Poisson's ratio, u_{12}	**0.28**
Poisson's ratio, u_{31}	**0.28**
Poisson's ratio, u_{23}	**0.15**
Shear moduli, G_{12} (GPa)	**4.7**
Shear moduli, G_{13} (GPa)	**4.7**
Shear moduli, G_{23} (GPa)	**4.261**
Longitudinal tensile strength, X_t(MPa)	**1550**
Longitudinal compressive strength, X_c(MPa)	**1090**
Transverse tensile strength, Y_t (MPa)	**59**
Transverse compressive strength, Y_c (MPa)	**207**
Longitudinal Shear Strength, S_{12} (MPa)	**128**
Transverse Shear Strength, S_{23} (MPa)	**75**
Longitudinal Tensile Fracture Energy, G_{1c}^{T} (kJ/m^2)	**91.6**
Longitudinal Compressive Fracture Energy, G_{1c}^{C} (kJ/m^2)	**79.9**
Transverse Tensile Fracture Energy, G_{2C}^{T} (kJ/m^2)	**0.22**
Transverse Compressive Fracture Energy, G_{2C}^{C} (kJ/m^2)	**1.1**
Density, ρ (kg/m^3)	**1540**

Table 1: Material Properties of carbon fibre/epoxy laminate

3.2 Bullet types:

a) Shape and Size: Three types of bullet were used in the study mentioned below-

- Projectiles with varying internal nose-angle.
- Calibre Radius Head (CRH) of 1.5 and 2 which is the ratio of the radius of curvature of nose-part to the calibre (base diameter of bullet).
- Hemispherical.

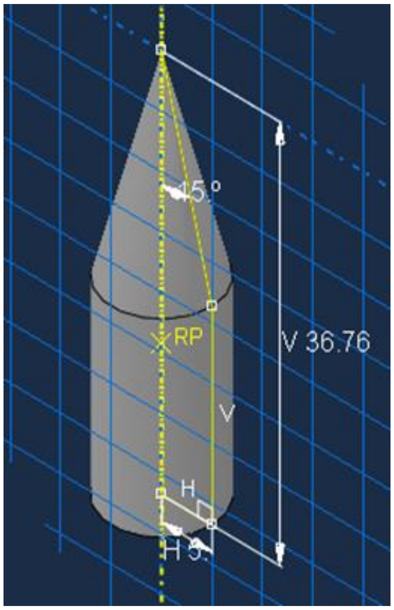

Figure 3.1: 30^0 nose-angle

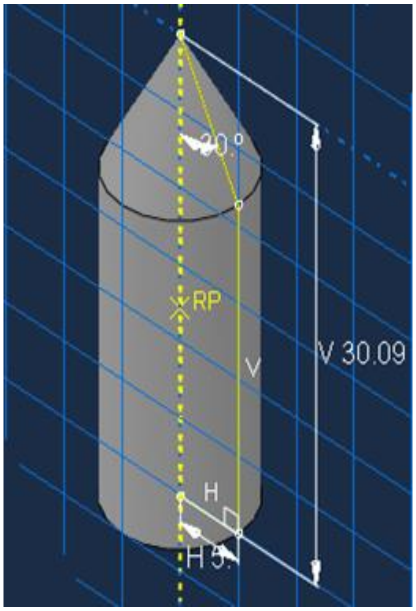

Figure 3.2: 60^0 nose-angle

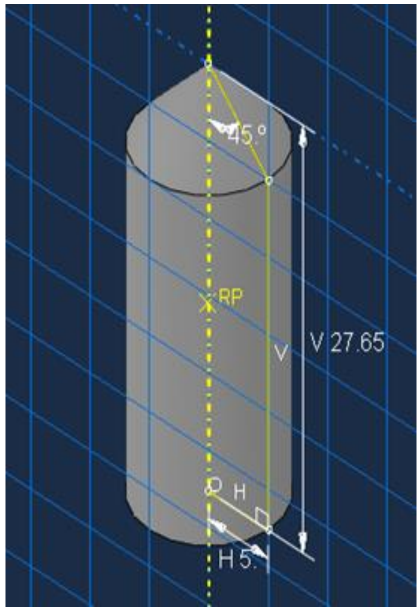

Figure 3.3: 90^0 nose-angle

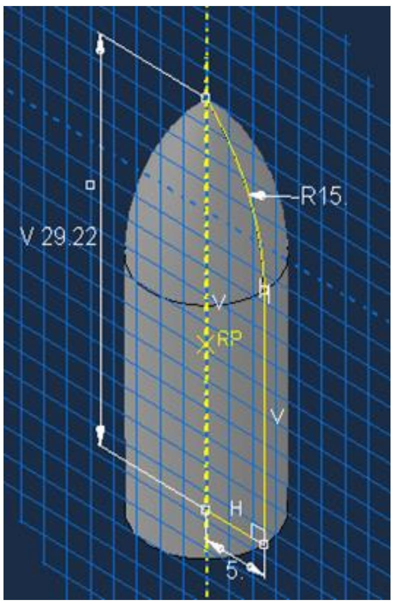

Figure 3.4: CRH 1.5

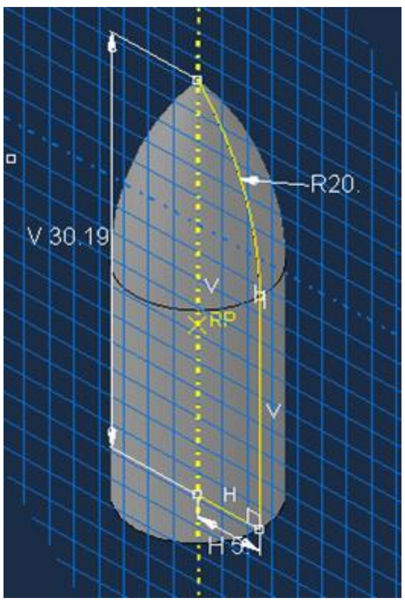

Figure 3.5: CRH 2.0

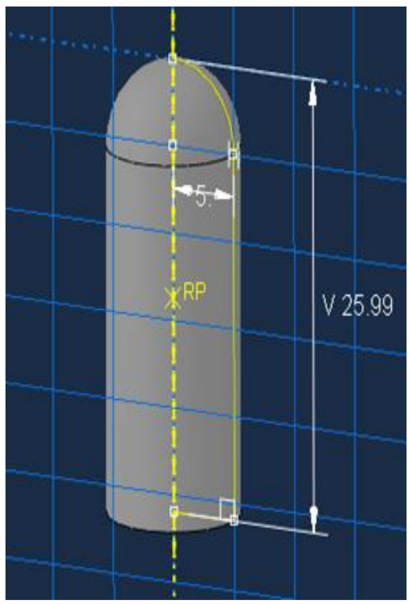

Figure 3.6: Hemispherical Shaped

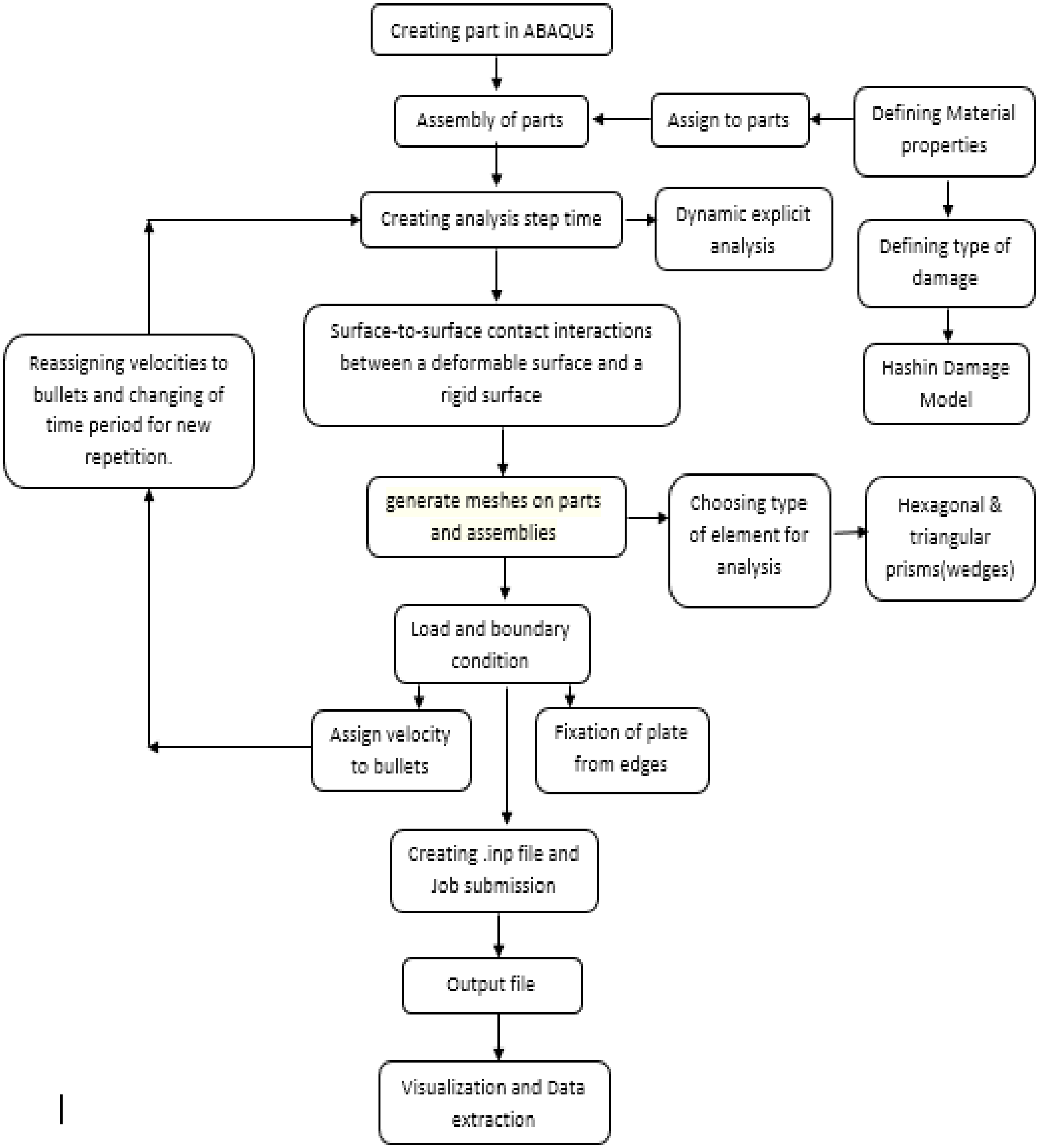

Figure 3.7 Flowchart of Numerical Model in ABAQUS

Chapter 4: Numerical Model

4.1 Analysis using ABAQUS

To evaluate the ballistic limit and kinetic energy loss of the CFRP sheet for different velocities, thicknesses, various bullet types and different span size, finite element analysis was performed. We have used different velocities in analysis ranging from velocities closer to ballistic limit to 300 m/s. ABAQUS/Explicit with Hashin Damage model was used for the analysis.

4.2 Modeling

Abaqus/CAE was used for modelling the CFRP sheet and different types of bullets. Different parts were made by using different modulus, after that, an input file was generated. This input file is submitted to Abaqus/Explicit to carry out the analysis. In Abaqus/CAE 'Part Module', the plate is modelled as 3D deformable solid and the bullet is modelled as 3D analytical rigid.

i. **Geometric Modeling:** For the numerical simulation, CFRP sheet of dimension 300mm x 300mm and 200mm x 200mm was considered. The number of layers taken was 5 and 10 with each being of 0.2mm with the corresponding thickness value of 1mm and 2mm respectively. The orientation of layers considered for each laminate was orthotropic as $[0/90]_{2s}$. There was two zone from the center to create fine mesh and reduce simulation time with better results as can be seen in fig 4.1.

   Projectiles were modeled of steel with a density of 7850 kg/m3 and a weight of 15 g for all the bullet type used in the analysis. The shape of the projectiles are hemispherical, ogive and conical having a diameter of 10mm for each of the bullet type.

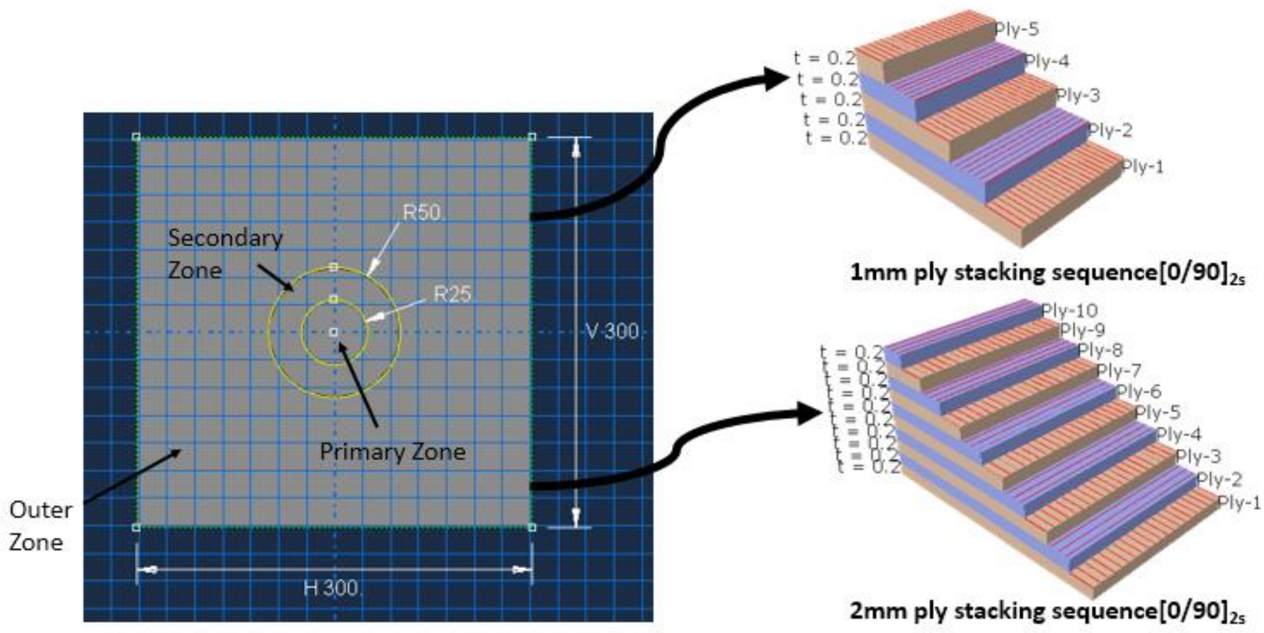

Figure 4.1 Geometric Design of CFRP Sheets used with different ply-stacking sequence.

ii. **Assembly:** A physical model is usually created by assembling different components. In Abaqus/CAE, the components which are assembled together are called part instances. So we can organize an Abaqus finite element model in terms of an assembly of part instances.

In 'Assembly Module', CFRP sheet and bullet are assembled relative to each other and a gap of 2mm is maintained initially to apply contact algorithm.

iii. **Step:** Abaqus/CAE creates an initial step at the beginning of any model's step sequence and calls it as 'Initial'. The initial step allows us to define the boundary conditions, predefined fields, and interaction algorithm which are initiated at the very beginning of the analysis.

The initial step is then followed by many more analysis steps. Each analysis step is related to a particular procedure that defines the analysis type to be performed during the step.

The total step time is being varied from 0.0002 sec to 0.02 sec for higher velocities to lower velocities, as low-velocity impact takes much time as compared to high-velocity impact.

iv. **Boundary Conditions:** Boundary conditions can be used for defining initial constraints and motion in the Abaqus/CAE model using the module create a load, create boundary condition and create predefined field under the module 'Load'.

In our model, we have used 'create boundary condition' for defining the boundary conditions at the edges of the CFRP sheet so that sheet is restricted to any movement or rotation at the edges.

ENCASTRE (U1=U2=U3=UR1=UR2=UR3=0) is being initialized in our model and for defining the velocity at the reference point (center of mass), we have used 'create predefined fields' and given the required velocity initially.

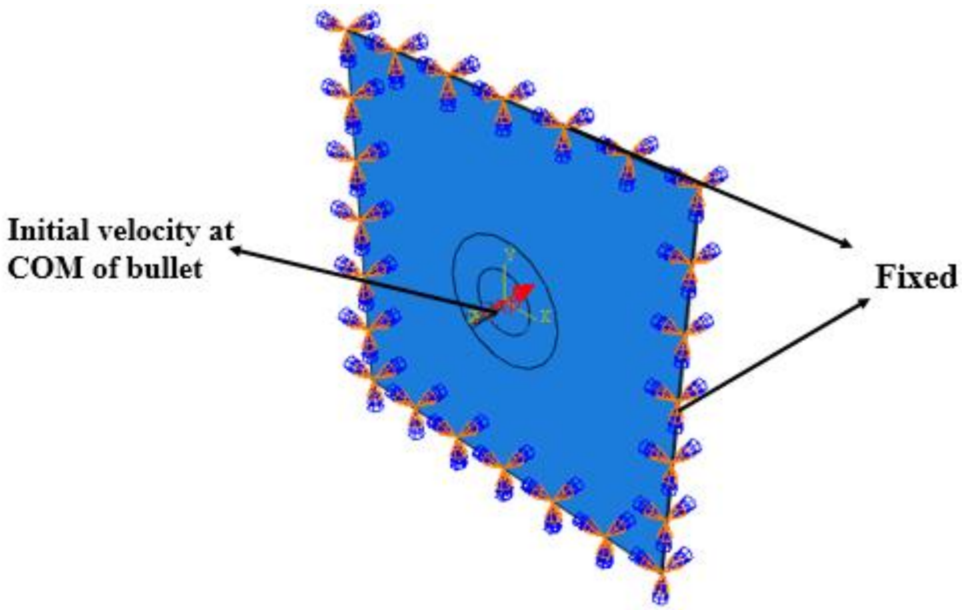

Figure 4.2: Image of boundary conditions applied in numerical simulations.

v. **Mesh Density and type of finite elements used:** The plate meshed with a different type of mesh size/density in a different region of the model as seen in figure 4.3

In Primary and Outer impact Zone, hexagonal elements (**SC8R:** An 8-node quadrilateral continuum shell, reduced integration) were used of size 1mm and 6mm respectively.

In the secondary impact zone, triangular elements (**SC6R**: A 6-node triangular continuum shell, reduced integration) were used of size 4mm.

The localized stiffness decrease because of internal damage can cause an excessive element distortion that could prompt to difficulties in numerical convergence, run slowly or even prematurely end the simulation. So the damage variable was adjusted to 0.99 to release some stiffness.

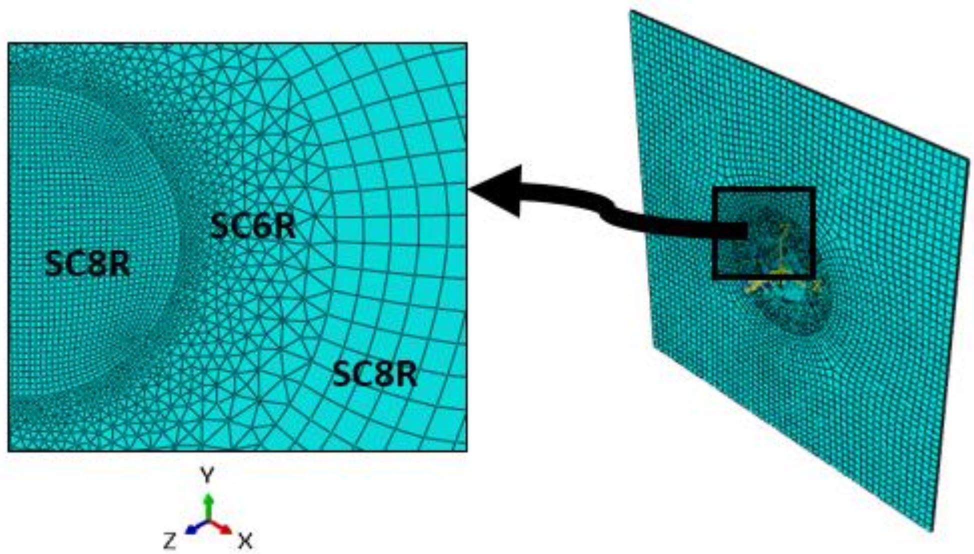

Figure 4.3: Types of mesh used in different zone with hexagonal and triangular elements.

vi. **Interaction Algorithm:** Interactions are step-dependent objects, which means that when you define them, you must indicate in which steps of the analysis they are active. Abaqus/CAE does not recognize mechanical contact between part instances or regions of an assembly unless that contact is specified in the Interaction module; the mere physical proximity of two surfaces in an assembly is not enough to indicate any type of interaction between the surfaces.

- **Understanding interactions:** There are various types of interaction option available but in our study, we have used Surface-to-surface contact. Surface-to-surface contact defines the interaction between two deformable bodies or either one deformable and rigid bodies.

There are various types of interaction properties that can be applied but we have used Contact Property. A contact interaction property can be defined as tangential behaviour (friction and an elastic slip) and normal behaviour (hard, soft, or damped contact). The friction coefficient between the composite laminates has been investigated in various literature [35-37]. This coefficient is a function of fibre orientation between contacted layers. In $0^0/0^0$ interface the valve is μ=0.2 but for adjacent 90^0 plies it is 0.8. Similarly, the coefficient between the surface of metal impactor and composite plate the valve used is 0.3.

Chapter 5: Experiment

5.1 Experimental setup: The experiments have been performed at Indian Institute of Technology, Roorkee. The experiments were conducted on a pneumatic gun which can launch projectile upto speed of 300m/s with the help of pressure chamber. The length of the barrel was considered 21m to obtain acceleration to achieve the required velocity. The angle of impact was considered to be normal and CFRP sheet is mounted on the mounting plate and clamped at the edges so that it can't move when projectile hits the target.

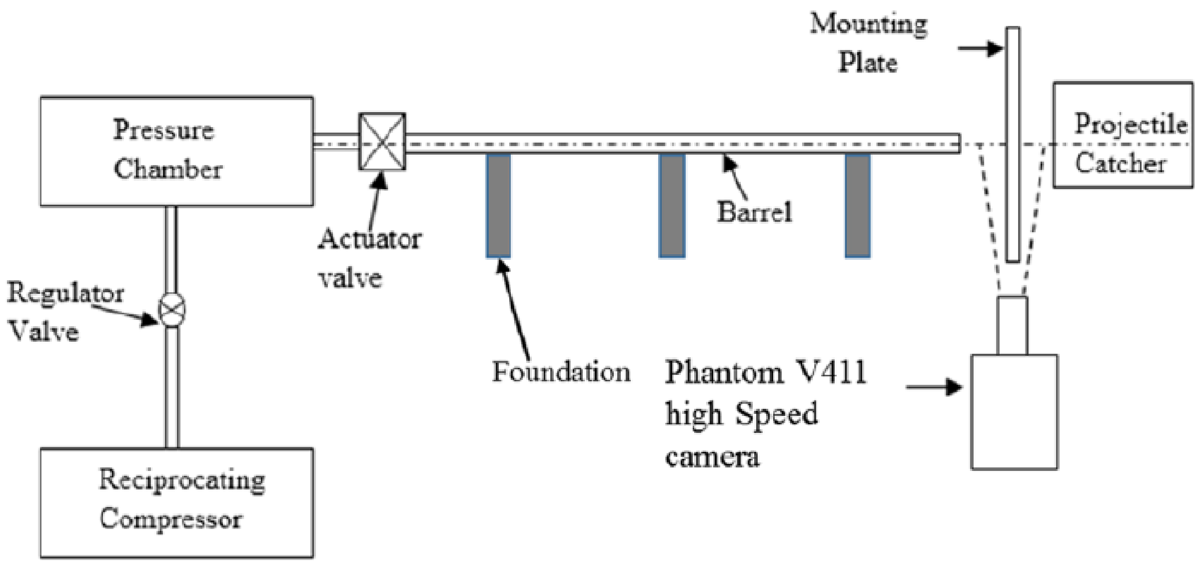

Figure 5.1 Pneumatic Gun experimental setup

Figure 5.2 Onsite experimental setup in IIT Roorkee

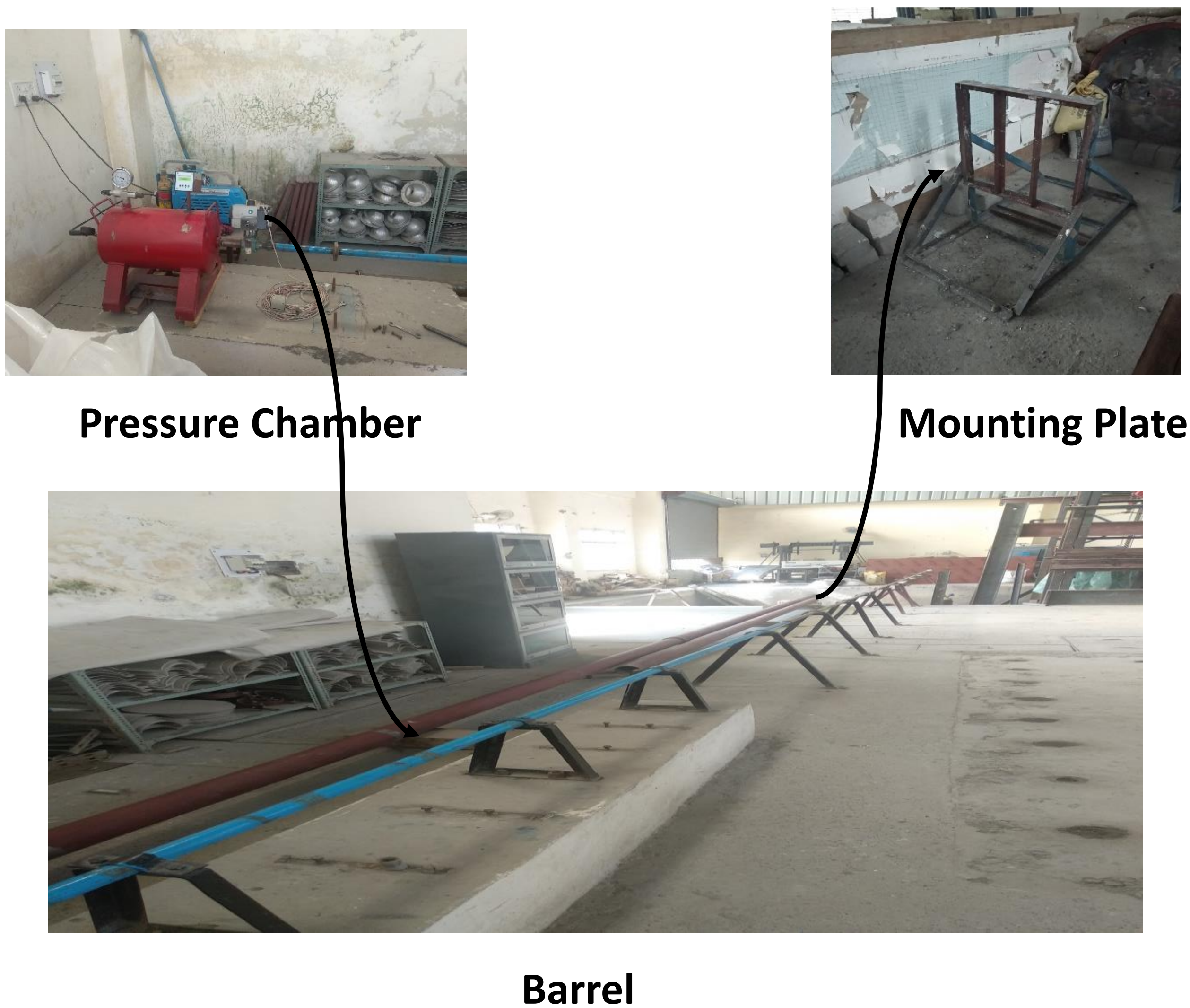

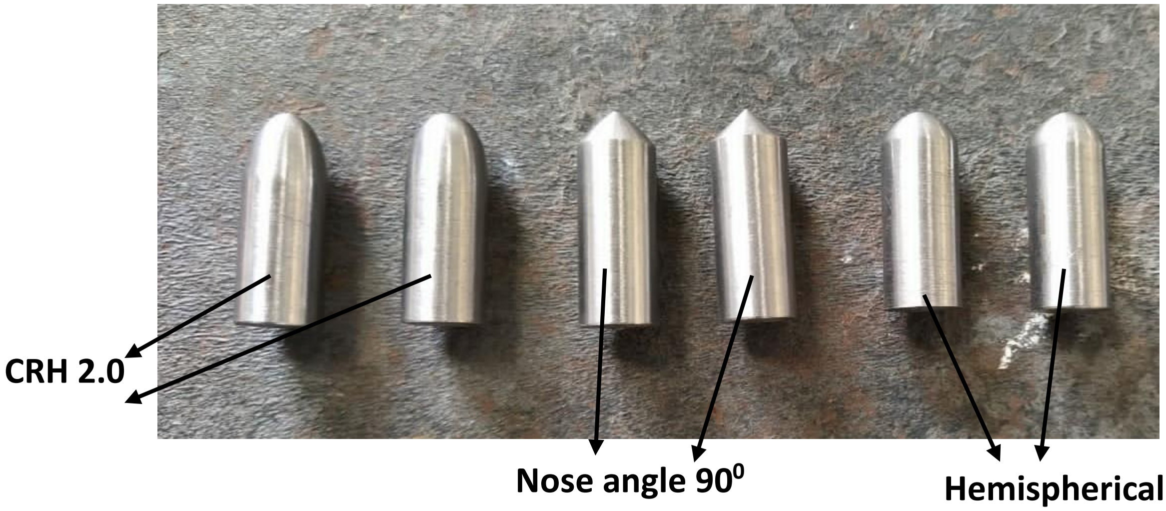

Figure 5.3 Types of bullets used for experiment

5.2 Damage analysis of target:

According to the images obtained of the sheet after experiments, it has been found that rear face has more damage as compared to the front face. For 1mm thickness sheets impacted with higher velocities, a clear notch type of damage has been observed taking that notch part away from sheet creating a clear hole in the sheet. For 2mm thickness sheets, major damage has been done on the rear part and more fiber breaking at the rear part of sheet too creating a bigger damage area.

Impact Velocity = 113m/s, Residual velocity = 89m/s

Front view, T=2mm

(a)

Rear view, T=2mm

(b)

Impact Velocity = 125m/s, Residual velocity = 94m/s

Front view, T=1mm

(c)

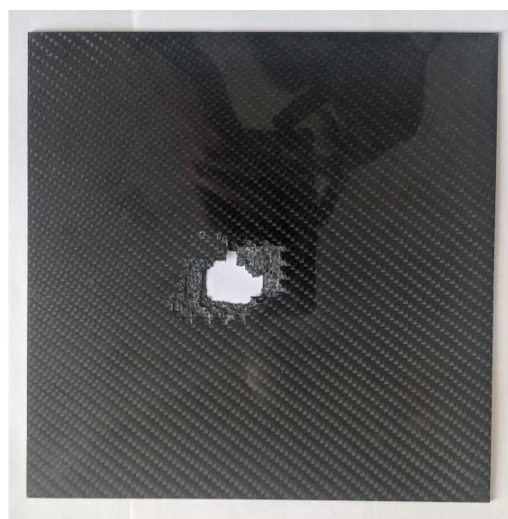

Rear view, T=1mm

(d)

Figure 5.4 Front and rear view of CFRP sheet impacted with hemispherical bullet for different thickness as shown in (a), (b), (c) and (d).

Impact Velocity = 112m/s, Residual velocity = 88m/s

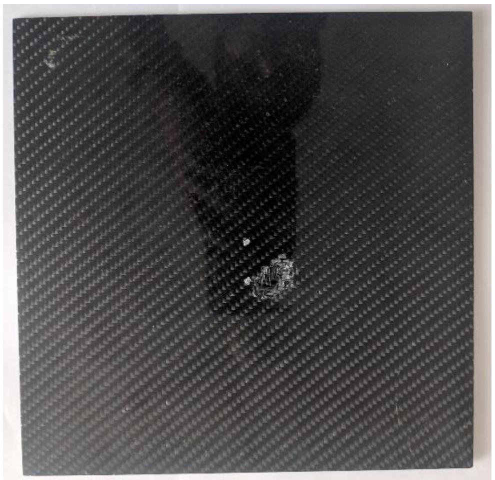

Front view, T=2mm

(a)

Rear view, T=2mm

(b)

Impact Velocity = 110m/s, Residual velocity = 99m/s

Front view, T=1mm

(c)

Rear view, T=1mm

(d)

Figure 5.5 Front and rear view of CFRP sheet impacted with CRH 2.0 bullet for different thickness as shown in (a), (b), (c) and (d).

Impact Velocity = 113m/s, Residual velocity = 88m/s

Front view, T=2mm

(a)

Rear view, T=2mm

(b)

Impact Velocity = 150m/s, Residual velocity = 125m/s

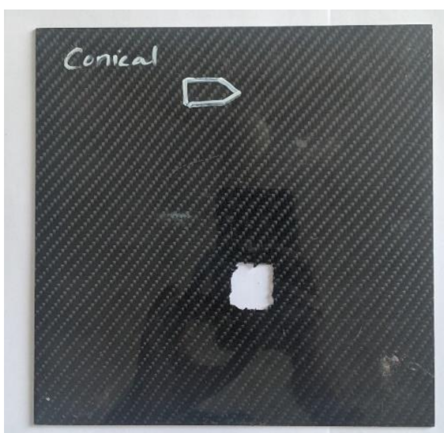

Front view, T=1mm

(c)

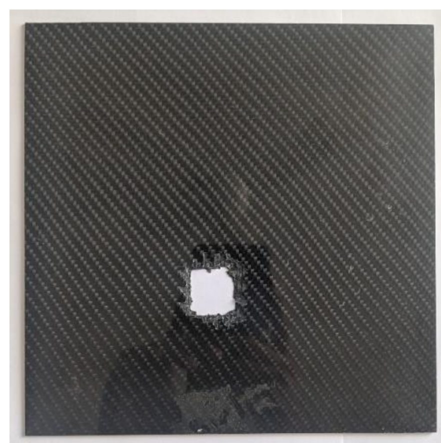

Rear view, T=1mm

(d)

Figure 5.6 Front and rear view of CFRP sheet impacted with conical bullet for different thickness as shown in (a), (b), (c) and (d).

Chapter 6: Results and Discussion

As explained in the above section, the FE model has been created for our specified problem. In this section, some of the perforation characteristics like ballistic limit velocity, residual velocity and loss in kinetic energy or perforation energy has been discussed obtained by FE model also perforation characteristics vary depending on the projectile properties, target sheets and impact velocities.

For the design of protective structures, perforation is taken into consideration. So, we have shown some perforations of CFRP sheets target by different type of bullets. The models image can be seen below:

CFRP Sheets perforated by Hemispherical shaped bullet at initial velocity of 200m/s

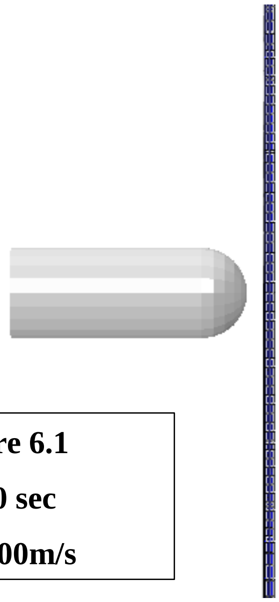

Figure 6.1

T= 0 sec

V = 200m/s

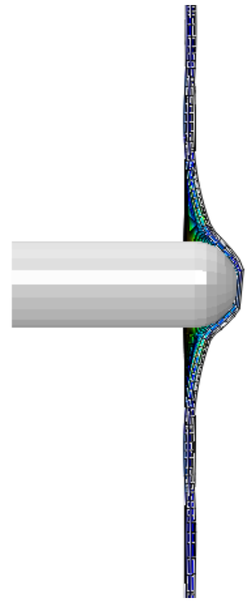

Figure 6.2

T= 0.00004 sec

V = 195.78 m/s

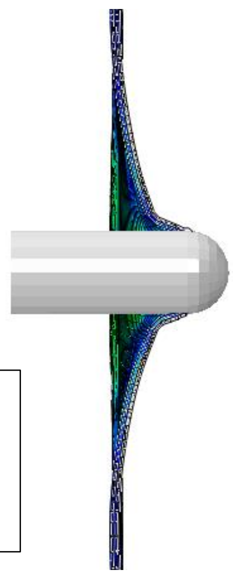

Figure 6.3

T=0.00008 sec

V = 193.76 m/s

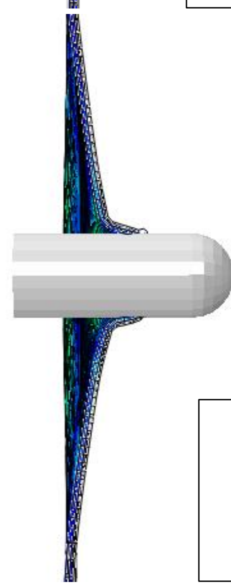

Figure 6.4

T=0.00011 sec

V = 193.25 m/s

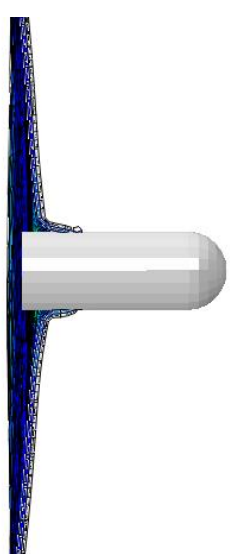

Figure 6.5

T=0.00015 sec

V = 192.39 m/s

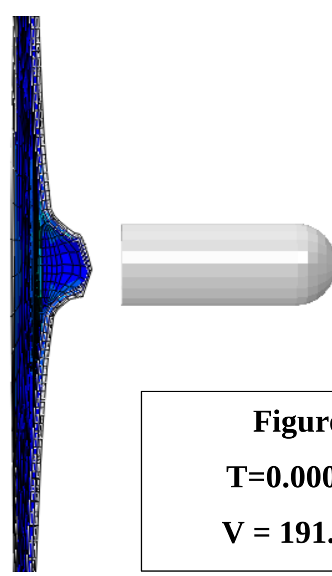

Figure 6.6

T=0.00021 sec

V = 191.62 m/s

CFRP Sheets perforated by nose angle of 30^0 bullet at initial velocity of 95m/s

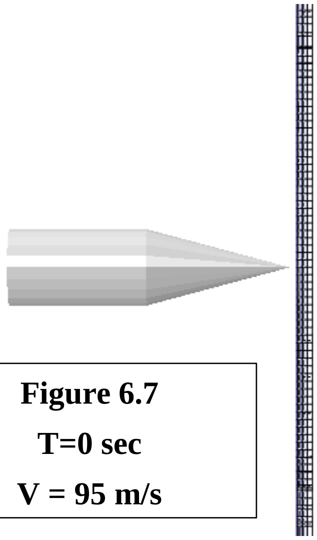

Figure 6.7
T=0 sec
V = 95 m/s

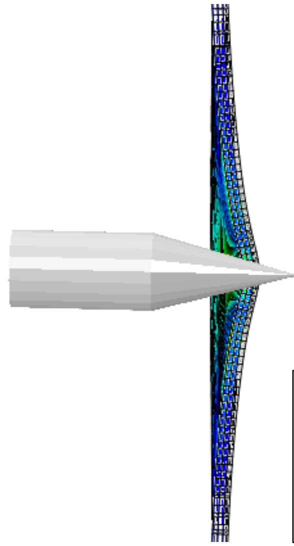

Figure 6.8
T=0.000135 sec
V = 80.85 m/s

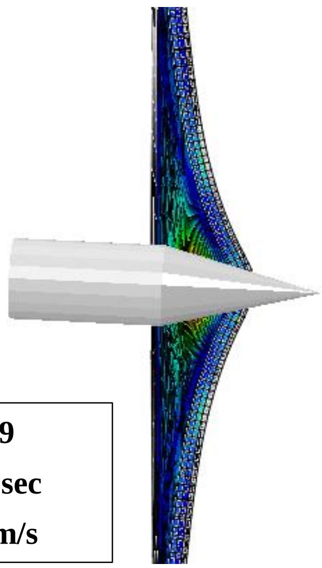

Figure 6.9
T=0.00026 sec
V = 59.08 m/s

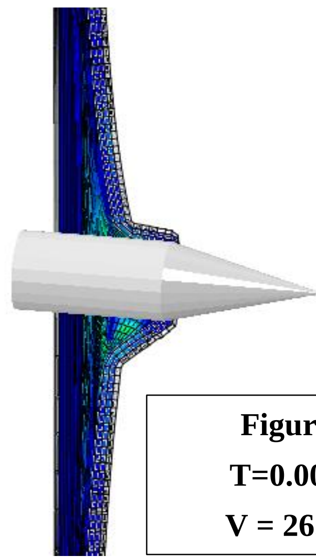

Figure 6.10
T=0.0006 sec
V = 26.10 m/s

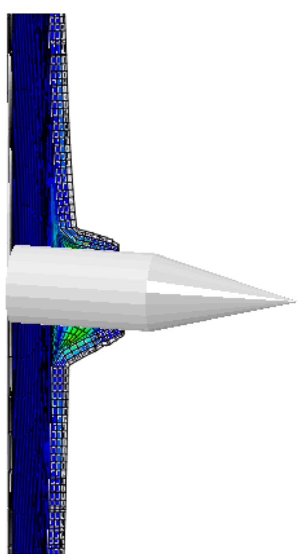

Figure 6.11
T=0.0009 sec
V = 10.94 m/s

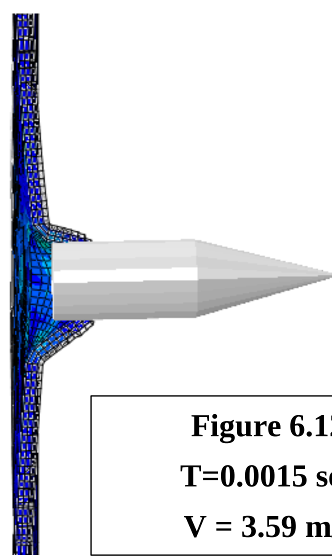

Figure 6.12
T=0.0015 sec
V = 3.59 m/s

CFRP Sheets perforated by nose angle of 60^{0} bullet at initial velocity of 75m/s

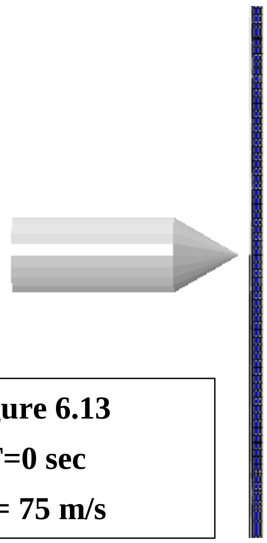

Figure 6.13
T=0 sec
V = 75 m/s

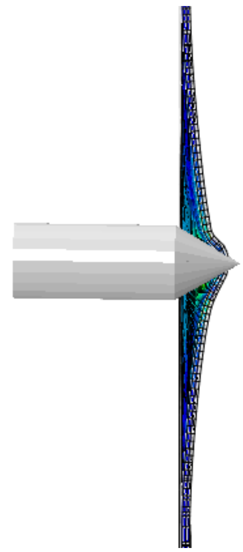

Figure 6.14
T=0.00013 sec
V = 69.95 m/s

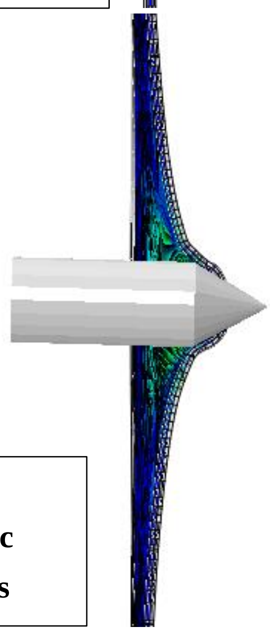

Figure 6.15
T=0.00025 sec
V = 61.61 m/s

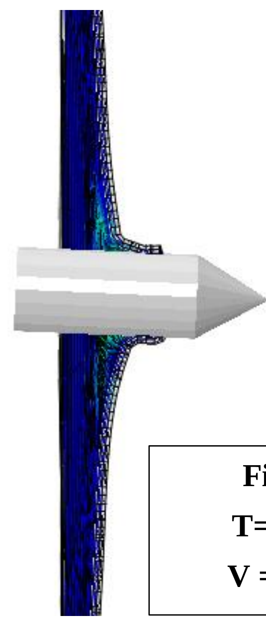

Figure 6.16
T=0.0004 sec
V = 54.58 m/s

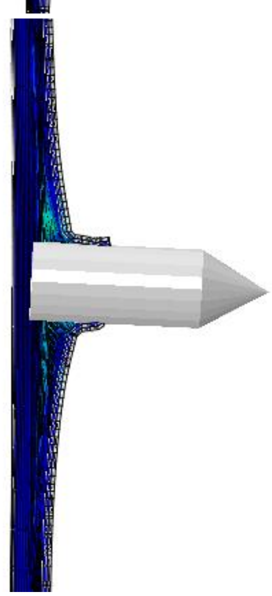

Figure 6.17
T=0.00055 sec
V = 50.07 m/s

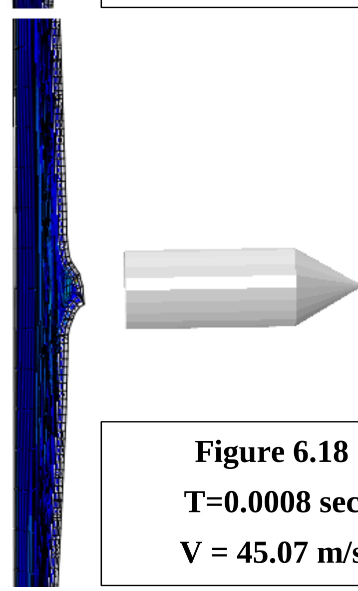

Figure 6.18
T=0.0008 sec
V = 45.07 m/s

CFRP Sheets perforated b ogive shaped bullet of CRH 2.0 at initial velocity of 150m/s

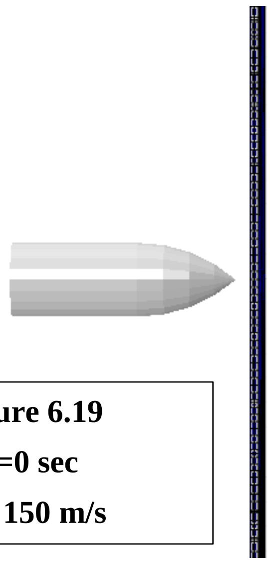

Figure 6.19
T=0 sec
V = 150 m/s

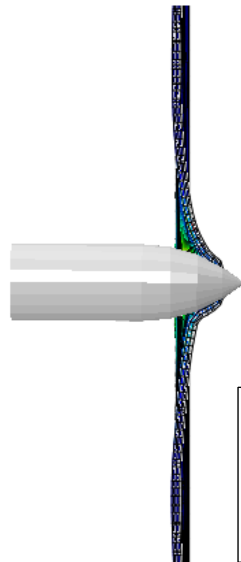

Figure 6.20
T=0.000075 sec
V = 145.96 m/s

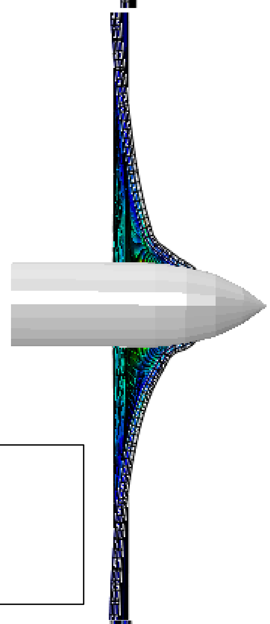

Figure 6.21
T=0.00014 sec
V = 141.02 m/s

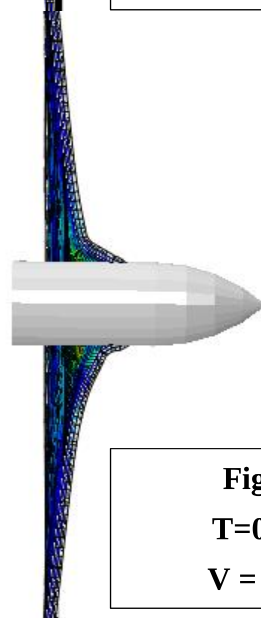

Figure 6.22
T=0.0002 sec
V = 138.5 m/s

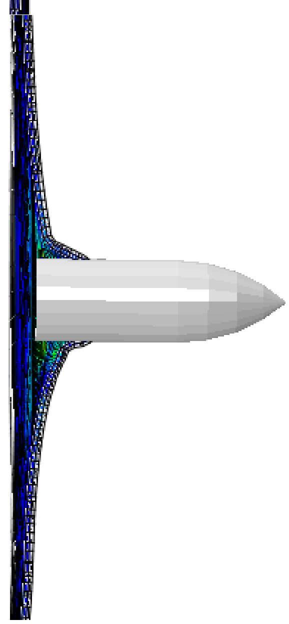

Figure 6.23
T=0.00025 sec
V = 136.65 m/s

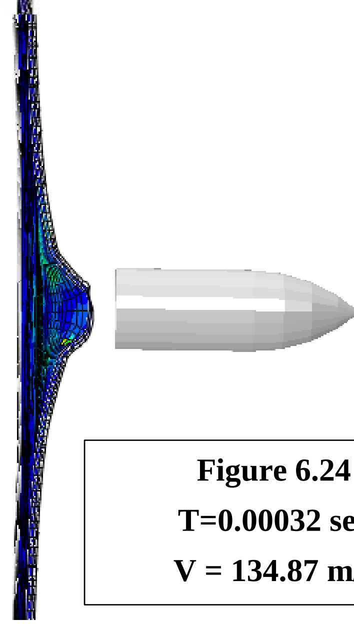

Figure 6.24
T=0.00032 sec
V = 134.87 m/s

6.1 Ballistics Limit Velocity: The ballistic limit or ballistic limit velocity is defined as the minimum velocity beyond which a particular projectile perforates a particular target plate and below it will not or it can be defined as the maximum velocity where a particular projectile get struck in a particular target plate.

In our FE model, we have calculated the ballistic limit velocity by taking the average of minimum perforation velocity and maximum struck velocity for more precise results. Thus, we have obtained the ballistic limit for the span (300x300) mm and (200x200) mm are presented in the tables below-

Ballistic Limit Velocity (m/sec)	Hemispherical		Nose Angle						CRH			
			30^0		60^0		90^0		**1.5**		**2**	
	1mm	2mm	1mm	2mm	1mm	2mm	1mm	2mm	1mm	2mm	1mm	2mm
	61.25	101.25	56.25	92	58.75	95.75	61.25	98	61.25	97	57	93.75

Table 2: Numerical simulation results of ballistic limit velocity for span (300 x 300) mm

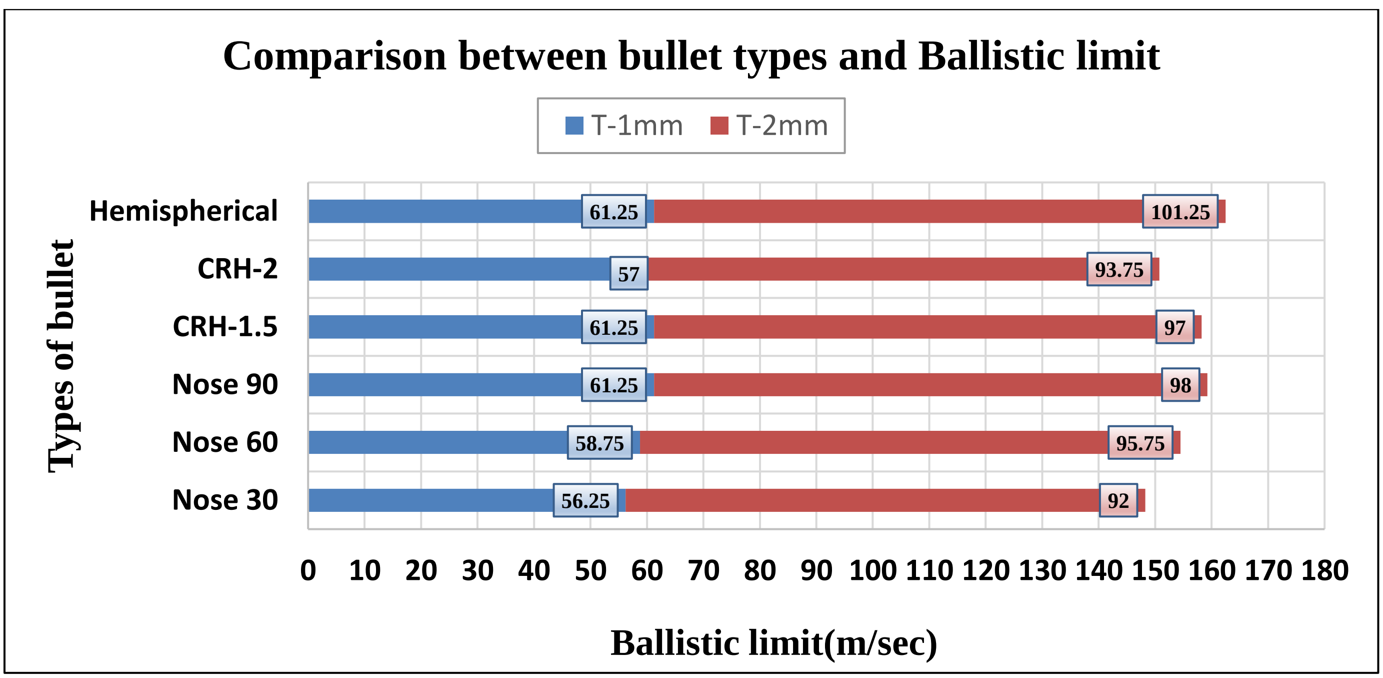

Ballistic Limit Velocity (m/sec)	Hemispherical		Nose Angle						CRH			
			30^0		60^0		90^0		**1.5**		**2**	
	1mm	2mm	1mm	2mm	1mm	2mm	1mm	2mm	1mm	2mm	1mm	2mm
	56.25	96.25	55.75	92.5	56.25	96.25	56.75	96.25	-	-	57.5	-

Table 3: Numerical simulation results of ballistic limit velocity for span (200 x 200) mm

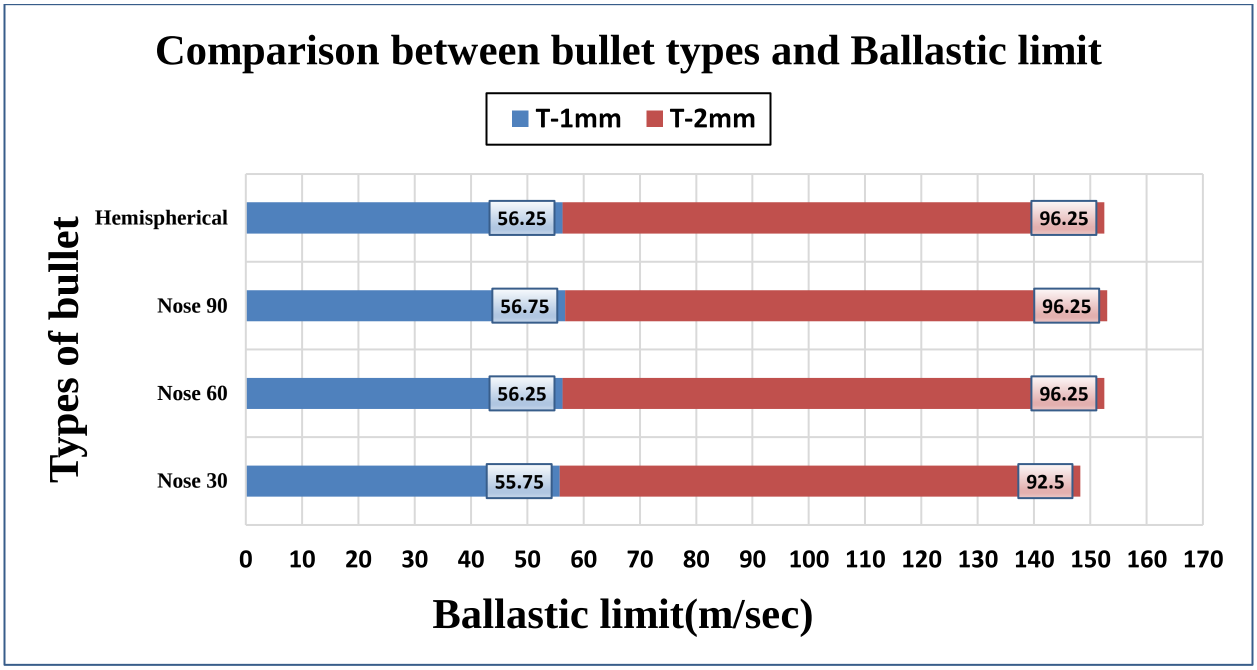

From the simulations, it has been found that as plate thickness increases perforation time also increases and at given thickness as impact velocity increases perforation time decreases. The ballistic limit was found to increase with a decrease in projectile nose angle like from 90^0 to 60^0 it was **4.26%** and from 60^0 to 30^0 it was **4.44%.** Similarly for the increase in CRH valve sharpness will increase which will result in a decrease in ballistic limit by **7.46%** for the span (300x300) mm.

The almost same trend was observed for span (200x200) mm, Ballistic limit is increasing with the increase in nose angle but the percentage increase is quite less. The ballistic limit value is less in smaller span in most cases, this is maybe due to the fact that resistance of bigger span is more in compared to the smaller ones.

6.2 Residual velocity: It can be defined as exiting velocity or terminal velocity when a projectile hits the target and completely passes through it and attains a terminal velocity which is constant as no forces are acting on the projectile in the direction of the motion it is known as residual velocity.

It is being observed during the simulation that residual velocity increases as the impact velocity increase for the impact velocities higher than the ballistic limit and with increases in thickness of the target sheet, residual velocity decreases. As we keep increasing the impact velocity the residual velocity will come closer to the impact velocity but in any case, it will always be less than impact velocity. As we have then decreased the span size but no significant change was observed, trends were almost the same.

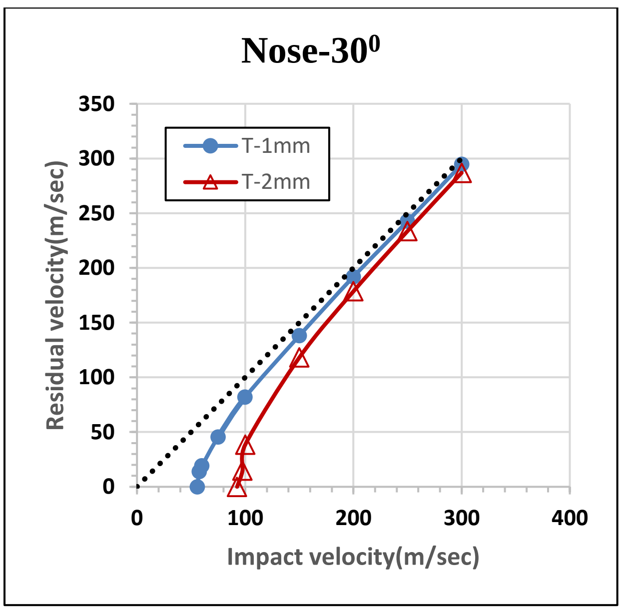

Figure 6.25 Residual velocity as a function of Impact velocity when impacted with 30^0 nose-angle bullet for (200 x 200)mm span

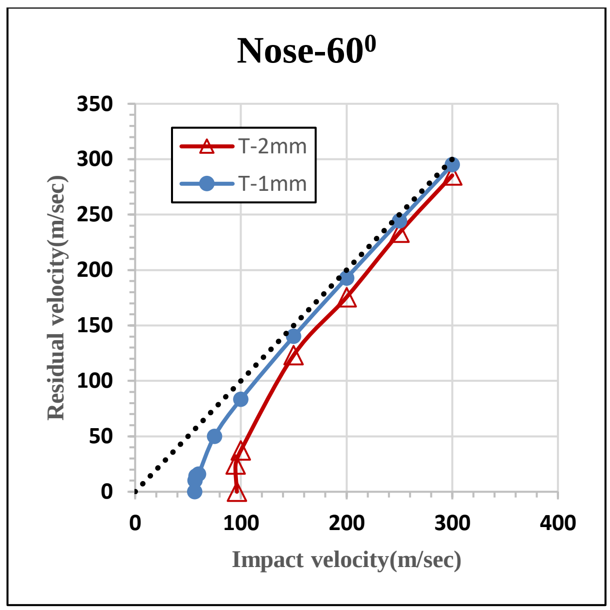

Figure 6.26 Residual velocity as a function of Impact velocity when impacted with 60^0 nose-angle bullet for (200 x 200) mm span.

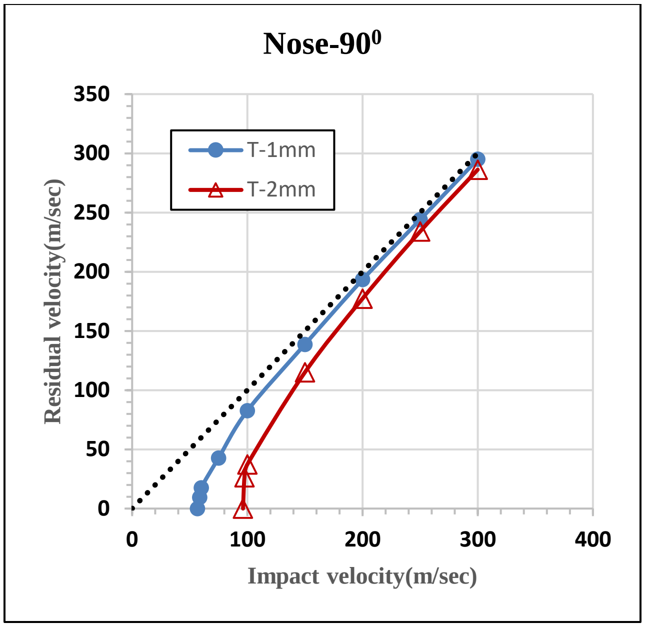

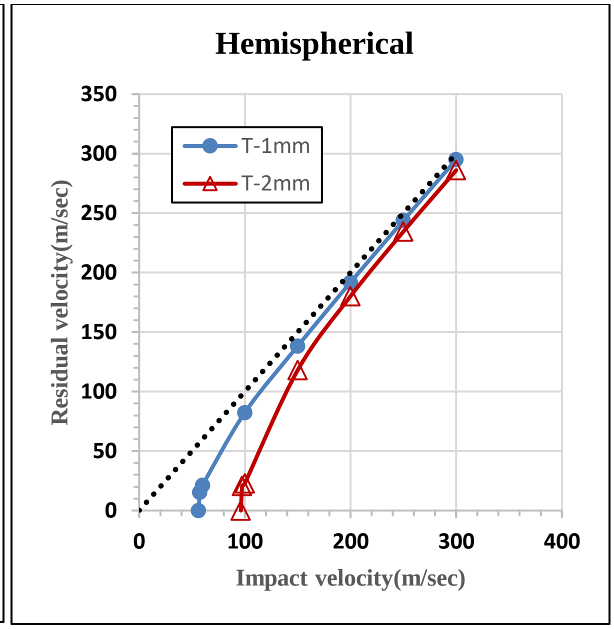

Figure 6.27 Residual velocity as a function of Impact velocity when impacted with 90^0 nose-angle bullet for (200 x 200)mm span.

Figure 6.28 Residual velocity as a function of Impact velocity when impacted with hemispherical shaped bullet for (200 x 200)mm span.

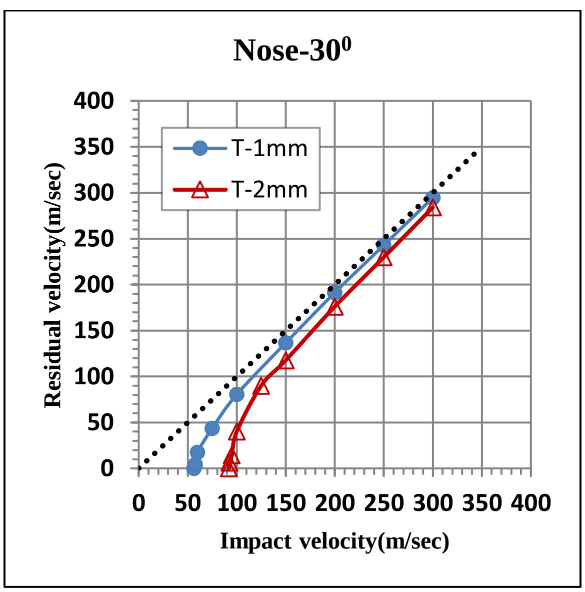

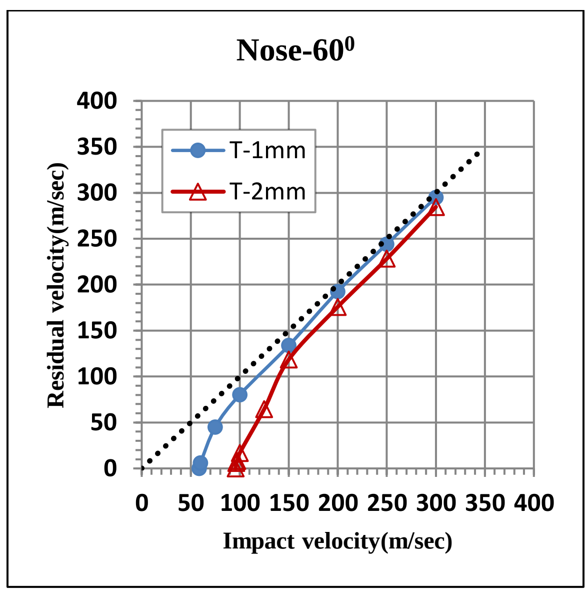

Figure 6.29 Residual velocity as a function of Impact velocity when impacted with 30^0 nose-angle bullet for (300 x 300) mm span.

Figure 6.30 Residual velocity as a function of Impact velocity when impacted with 60^0 nose-angle bullet for (300 x 300) mm span.

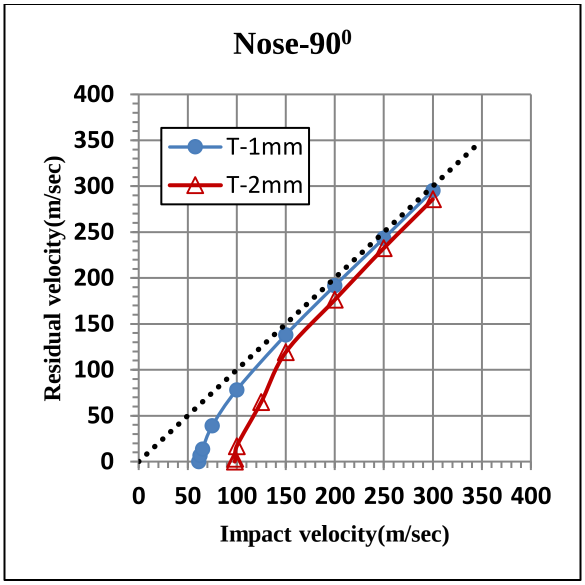

Figure 6.31 Residual velocity as a function of Impact velocity when impacted with 90^0 nose-angle bullet for (300 x 300) mm span.

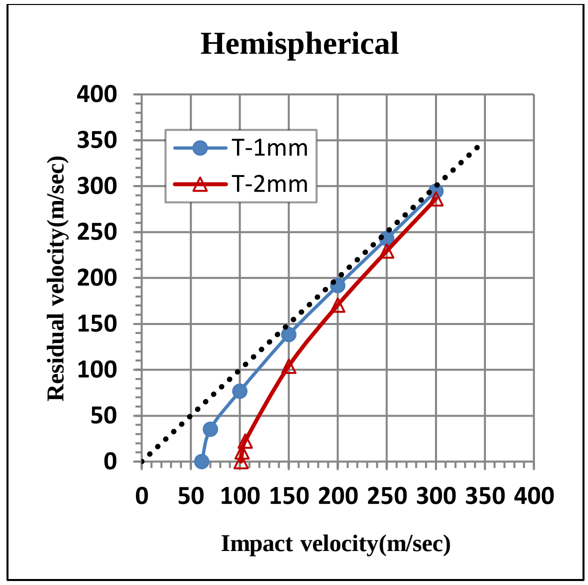

Figure 6.32 Residual velocity as a function of Impact velocity when impacted with hemispherical shaped bullet for (300 x 300) mm span.

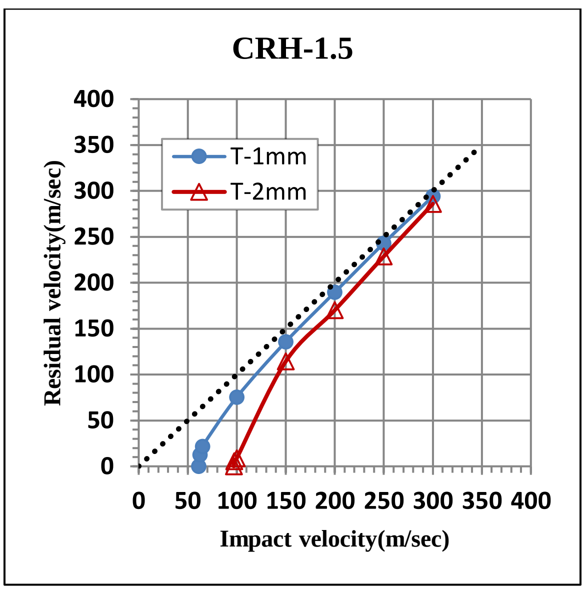

Figure 6.33 Residual velocity as a function of Impact velocity when impacted with Ogive shaped bullet of CRH 1.5 for (300 x 300) mm span.

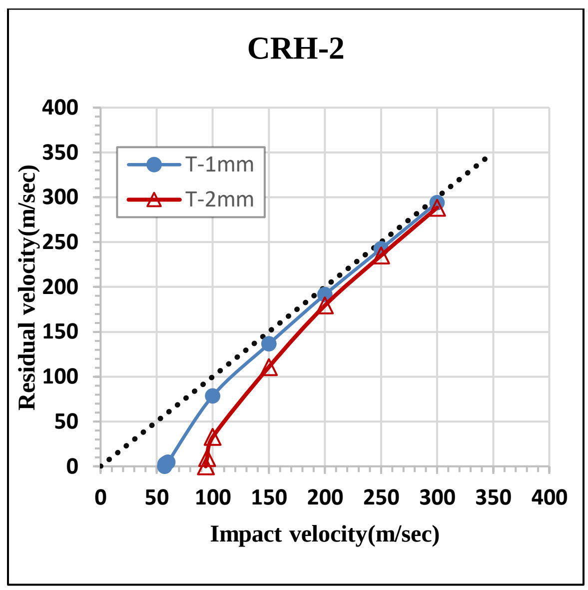

Figure 6.34 Residual velocity as a function of Impact velocity when impacted with Ogive shaped bullet of CRH 2.0 for (300 x 300) mm span.

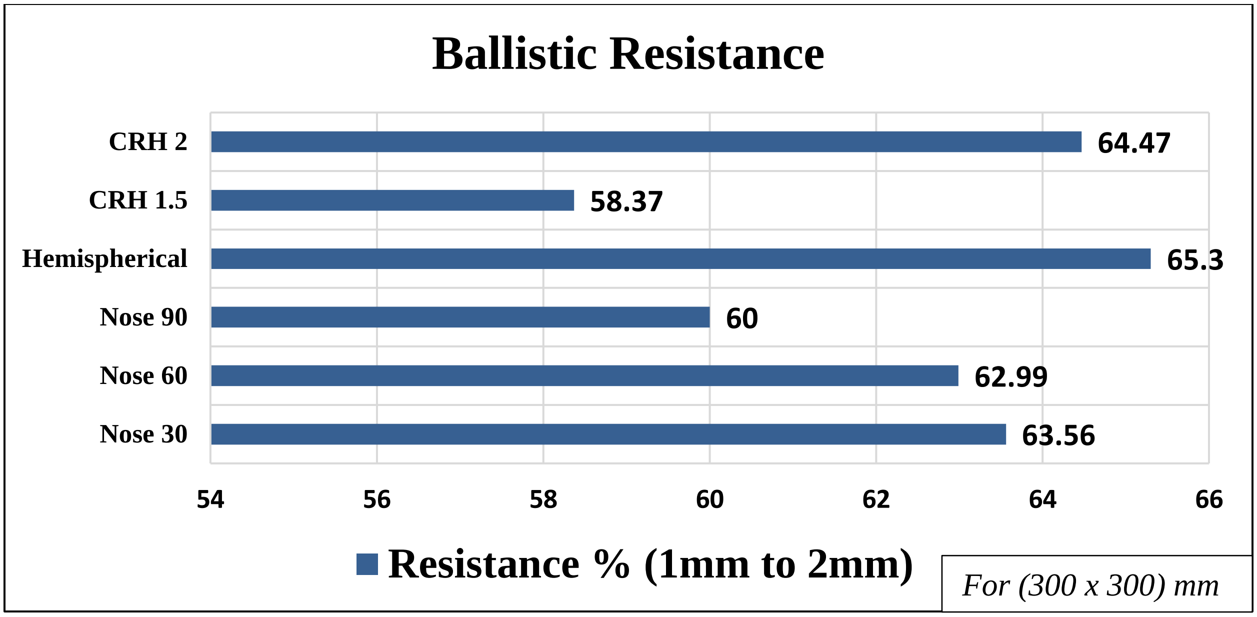

Figure 6.35 Ballistic Resistance by varying thickness for different bullet-types for span 300 x 300 mm.

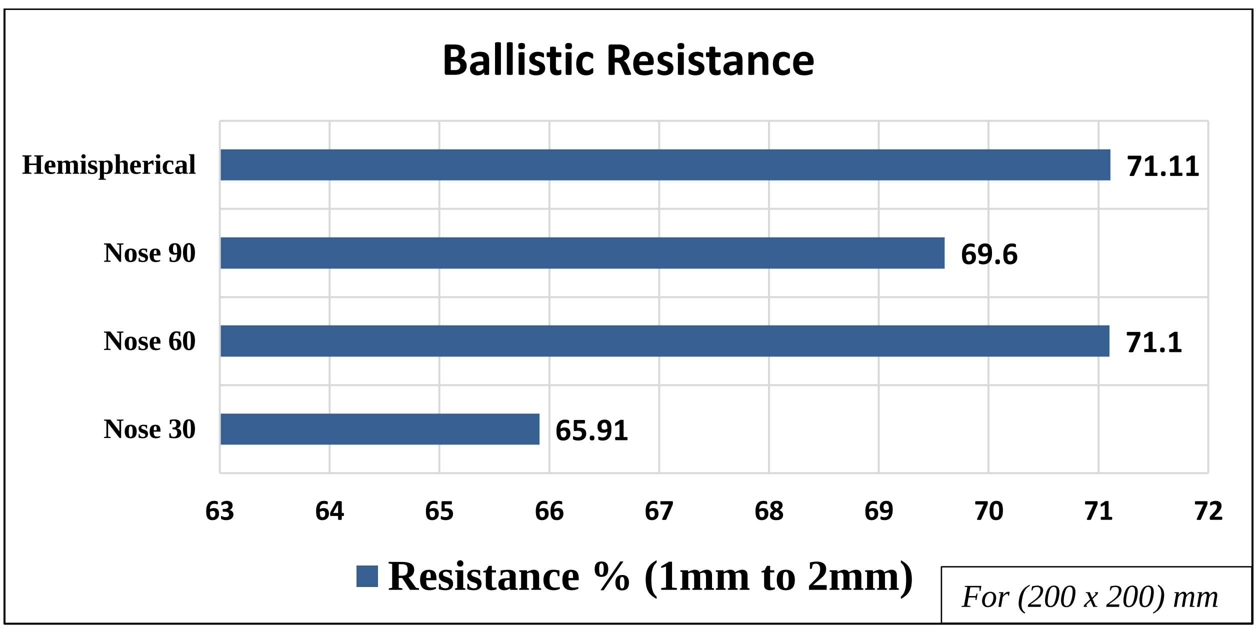

Figure 6.36 Ballistic Resistance by varying thickness for different bullet-types for span 200 x 200 mm.

6.3 Loss in Kinetic Energy: During a projectile impact, most of the kinetic energy is being dissipated and sometimes kinetic energy becomes completely zero when the initial Kinetic energy is less than the Perforation energy, it can be defined as the minimum energy required for the perforation of the sheet or can be understood as the threshold for a sheet to penetrate it.

Loss in Kinetic energy vs impact velocity is being plotted for all kind of projectiles used in simulation and it is been found that loss in Kinetic energy is for different impact velocities after ballistic limit is same. The curve varies around a fixed value by very less of a change and this fixed value is threshold or perforation energy. Increases in impact velocity does not necessarily increases or decreases the kinetic energy loss.

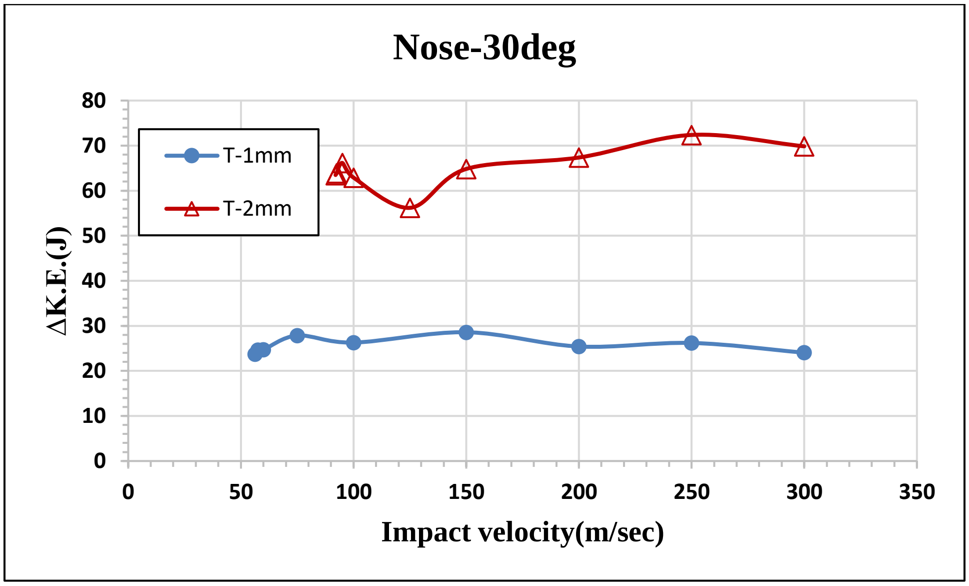

Figure 6.37 Energy loss as a function of Impact velocity for bullet of nose-angle 30^0

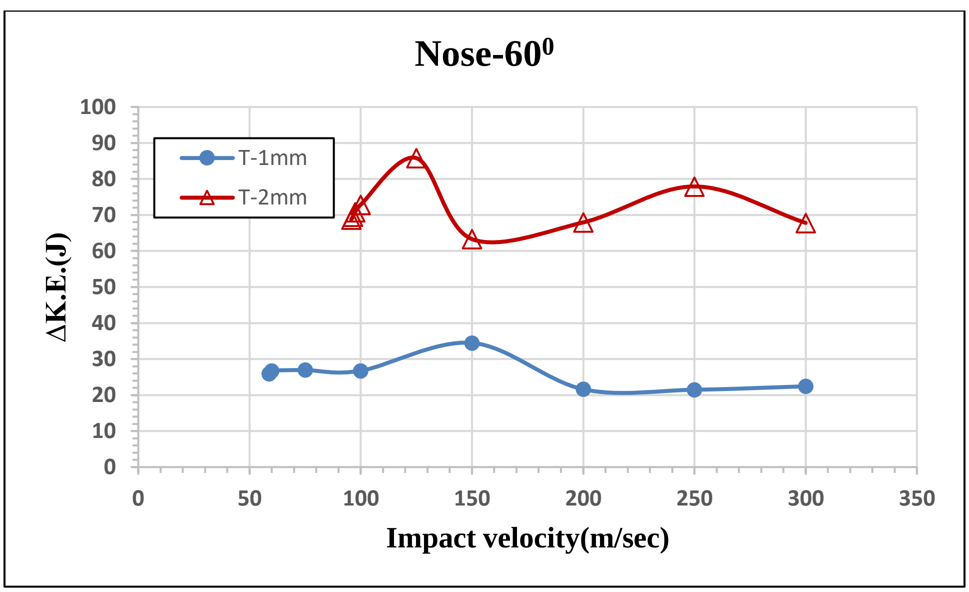

Figure 6.38 Energy loss as a function of Impact velocity for bullet of nose-angle 60^0

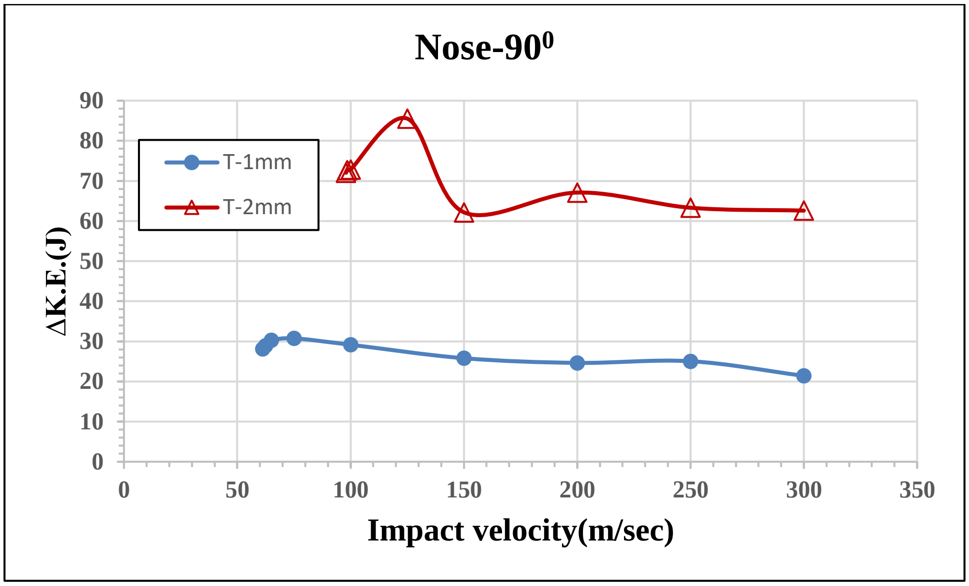

Figure 6.39 Energy loss as a function of Impact velocity for bullet of nose-angle 90^0

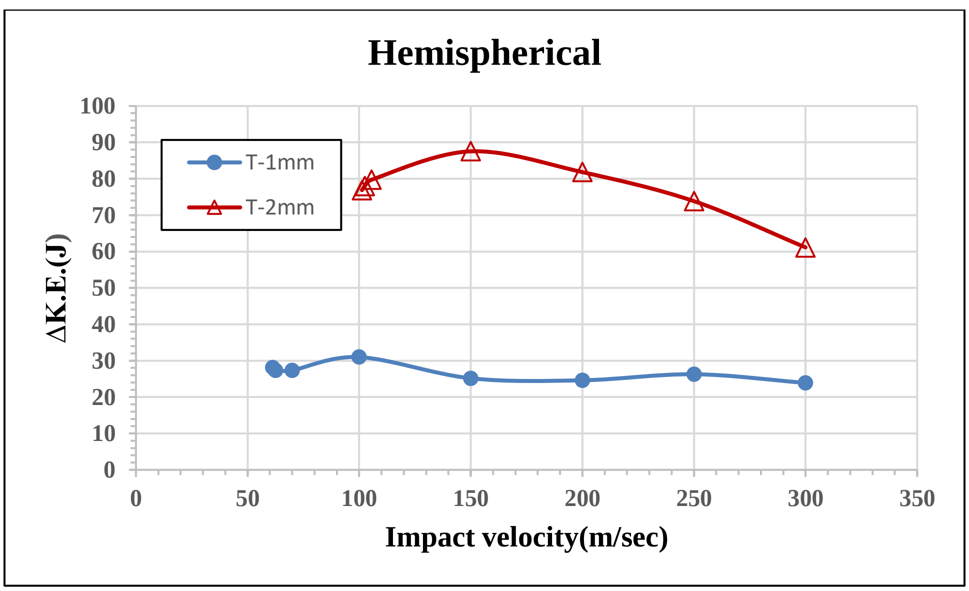

Figure 6.40 Energy loss as a function of Impact velocity for Hemispherical shaped bullet.

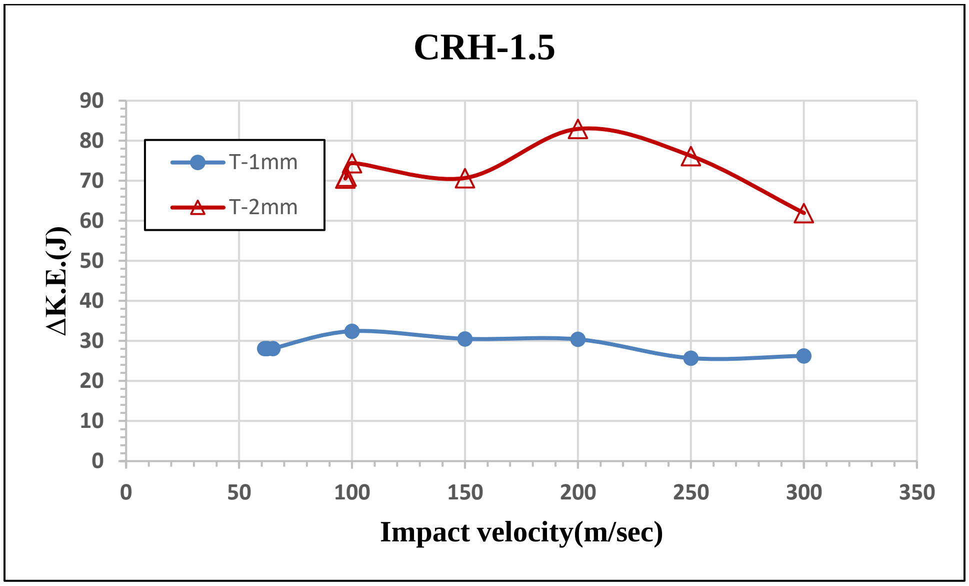

Figure 6.41 Energy loss as a function of Impact velocity for CRH 1.5

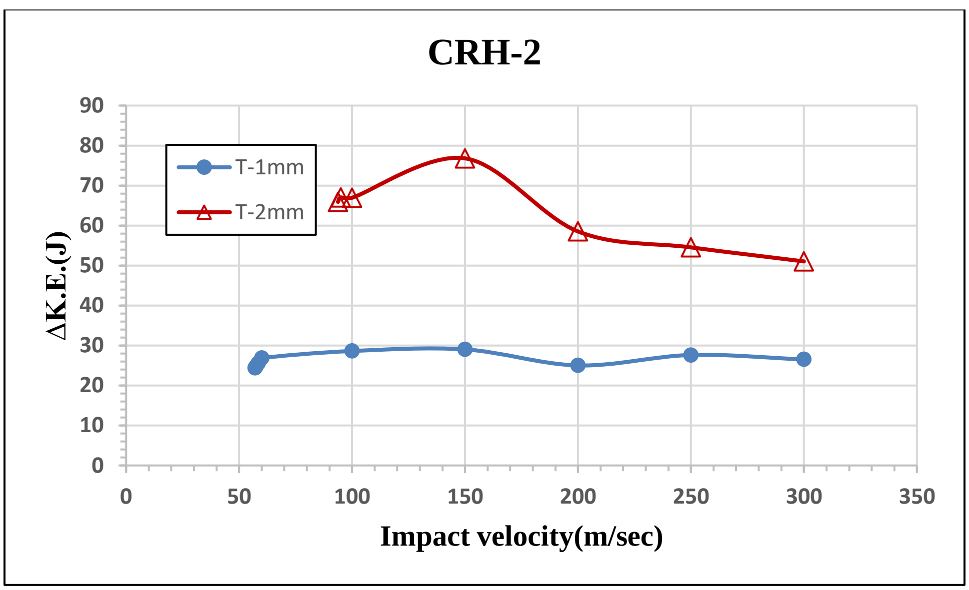

Figure 6.42 Energy loss as a function of Impact velocity for CRH 2.0

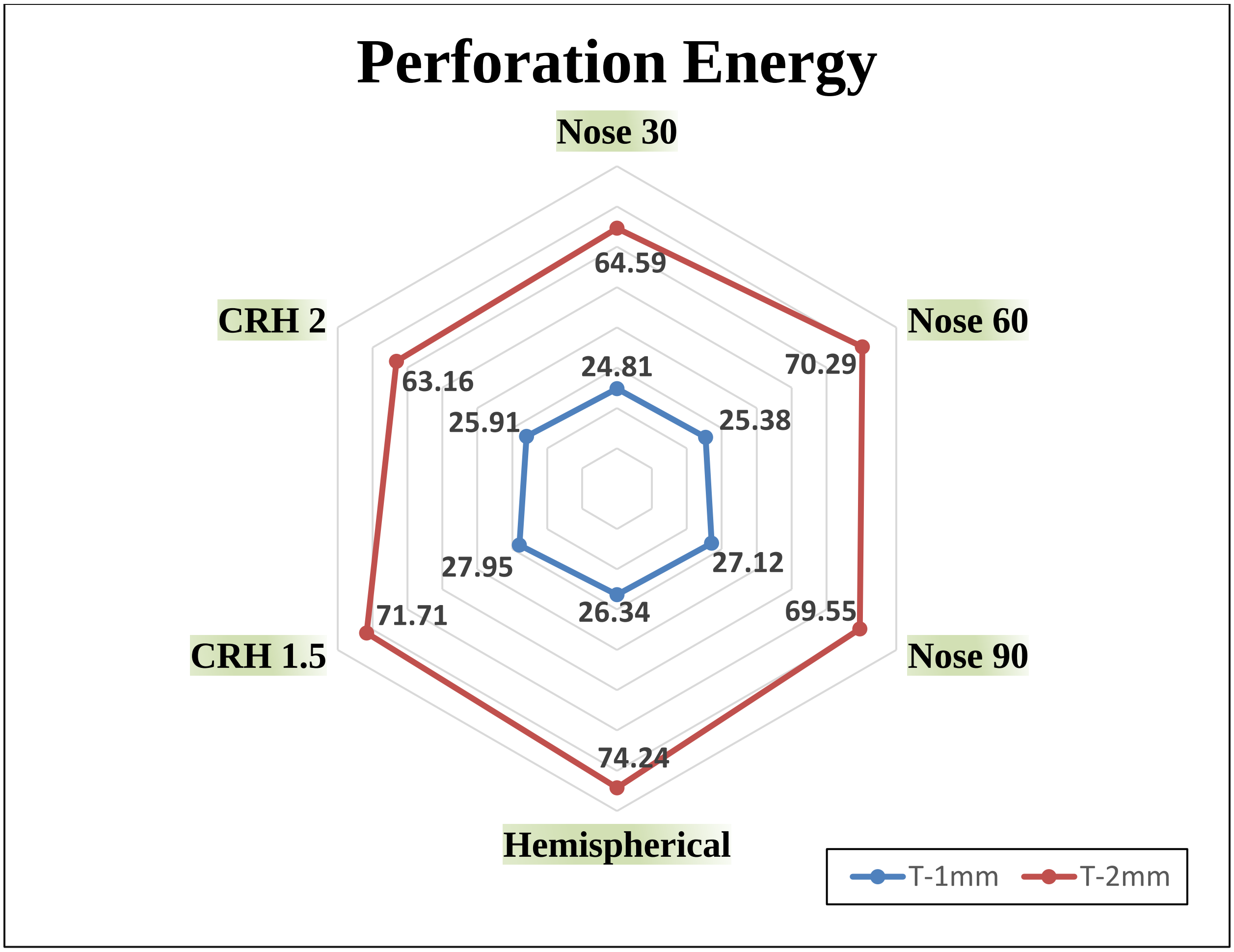

Span (300 x 300) mm

Figure 6.43 Perforation energy for different bullet types on span of 300 x 300 mm.

Perforation energy was found to be min. energy required to pass through the sheet by using average of energy loss curve as a function of impact velocity. The results of 300 x 300 mm span has been shown above in figure 6.41.

6.4 Results Validation:

Residual velocities has been calculated for 1mm and 2mm thickness specimens for different type of bullets from the experiments performed and these results are being compared to the simulation results obtained from the ABAQUS explicit software.

S. No.	Bullet Type	Thickness (mm)	Impact Velocity(m/s)	Residual Velocity(m/s)		%Error
				Simulation	Experimental	
1.	Conical- Nose 90^0	1	150	138.70	125	10.96
		2	113	54.80	88	32.72
2.	Hemispherical	1	125	110.23	94	17.26
		2	113	58.6	89	34.16
3.	CRH 2.0 (ogival)	1	110	85.64	99	13.49
		2	125	55.7	88	36.70

Table 4: Experimental and simulation results validation by %error calculation.

Chapter 7: Conclusion

In our study, a large number of impact tests were numerically modelled for large range of impact velocities to have better knowledge of perforation process and mechanism at the same time understanding the perforation characteristics. In spite of all this due to the complexity of the factors affecting them, more detailed study in the ballistic phenomenon is required to have better insight of the perforation mechanism which will be helpful for analytical and numerical modeling in impact analysis.

Till now the conclusion we have reached so far has been stated below as:

1. Effect by varying span: Slight changes were observed but changes were not significant.
2. Ballistic Limit: For 1mm, the ballistic limit was varying from 56.25m/s to 62.25m/s. For 2mm, the ballistic limit was found to vary from 92m/s to 101.25m/s. So, it has been found that nose-angle increases the perforation capacity decreases.
3. Loss in Kinetic Energy: As the velocity increases the kinetic energy of bullet increases but the net loss in kinetic energy with increase in velocity remains almost comparable.
4. Perforation Mechanism: Rear Damage was quite significant and large as compared to front damage and laminate/sheet damage is observed to be more at velocities closer to ballistic limit. The rear faces more damage because after the impact, the energy wave propagation increases as it travels through thickness, hence it faces more damages.
5. Validation of numerical model with experimental results: For 1mm, the experimental results were found to be close to the numerical damage model results from 10.96% to 17.26% for 1mm and for 2mm, the range was around 32.76% to 36.70%.

Future scope:

We are trying to validate the numerical results with the experimental test that has to be performed on CFRP sheets of different span, thickness, varying curvature of bullets to understand the dynamic characteristics response of composite fibres.

The analysis will help to give better in sight of the accuracy of damage model used in numerical simulations and its usage in coming future to understand the damage pattern.

References:

1. Hashin Z, Rotem A. A fatigue failure criterion for fiber-reinforced materials. J Compos Mater 1973;7:448–64.
2. Hashin, Z. (1980). Failure criteria for unidirectional fiber composites. Journal of applied mechanics, 47(2), 329-334.
3. Puck A, Schurmann H. Failure analysis of FRP laminates by means of physically based phenomenological models. Compos Sci Technol 1998;58(10):1045–67.
4. Shi, Y., Swait, T., & Soutis, C. (2012). Modelling damage evolution in composite laminates subjected to low velocity impact. *Composite Structures*, *94*(9), 2902-2913.
5. Sikarwar, R. S., Rajput, N. S., Velmurugan, R., & Naik, S. (2017). FE Analysis of impact on Kevlar/epoxy laminates with different orientations and thicknesses. *Materials Today: Proceedings*, *4*(2), 2599-2607.
6. Iqbal, M. A., Diwakar, A., Rajput, A., & Gupta, N. K. (2012). Influence of projectile shape and incidence angle on the ballistic limit and failure mechanism of thick steel plates. *Theoretical and Applied Fracture Mechanics*, *62*, 40-53.
7. Barbero, E.J. (2013). Finite Element Analysis of Composite Materials using Abaqus. Elasticity and Strength of Laminates, 102.
8. Pederson, Joy, "Finite Element Analysis of Carbon Fiber Composite Ripping Using ABAQUS" (2008). *All Theses*. 512. https://tigerprints.clemson.edu/all_theses/512
9. López-Puente, J., Zaera, R., & Navarro, C. (2008). Experimental and numerical analysis of normal and oblique ballistic impacts on thin carbon/epoxy woven laminates. *Composites Part A: applied science and manufacturing*, *39*(2), 374-387.
10. Kasano, H. (1999). Recent advances in high-velocity impact perforation of fiber composite laminates. *JSME International Journal Series A Solid Mechanics and Material Engineering*, *42*(2), 147-157.
11. Kasano, H. (2001). Impact perforation of orthotropic and quasi-isotropic CFRP laminates by a steel ball projectile. *Advanced Composite Materials*, *10*(4), 309-318.
12. Goldsmith, W., Dharan, C. K. H., & Chang, H. (1995). Quasi-static and ballistic perforation of carbon fiber laminates. *International Journal of Solids and Structures*, *32*(1), 89-103.
13. ABAQUS Explicit User’s manual, version 6.13 Edition.
14. ABAQUS v6.14. SIMULIA, Rising Sun Mills, 166 Valley Street, Providence, RI 02909.

IMAGE SOURCES:

Figure 1.1: https://forums.vwvortex.com/showthread.php?7654562-McLarent-P1-in-raw-carbon

Figure 1.2: https://www.icis.com/explore/resources/news/2009/12/14/9318715/boeing-s-787-dreamliner-has-some-impressive-environmental-credentials/

Figure 1.3: https://switchbladepaddles.com/products/acadia

Figure 1.4: https://www.energy.gov/eere/articles/timeline-path-lightweight-materials-cars-and-trucks